Feasibility of Fireball Trail Detection Using Ground-Based GPS Receivers

THESIS

Ian R. Moffett, 2d Lt, USAF

AFIT-ENP-MS-22-M-100

DEPARTMENT OF THE AIR FORCE
AIR UNIVERSITY

AIR FORCE INSTITUTE OF TECHNOLOGY

Wright-Patterson Air Force Base, Ohio

AFIT-ENP-MS-22-M-100

FEASIBILITY OF FIREBALL TRAIL DETECTION USING GROUND-BASED GPS RECEIVERS

THESIS

Presented to the Faculty

Department of Engineering Physics

Graduate School of Engineering and Management

Air Force Institute of Technology

Air University

Air Education and Training Command

in Partial Fulfillment of the Requirements for the

Degree of Master of Science in Applied Physics

Ian R. Moffett, B.S.

2d Lt, USAF

March 2022

AFIT-ENP-MS-22-M-100

FEASIBILITY OF FIREBALL TRAIL DETECTION USING GROUND-BASED GPS RECEIVERS

THESIS

Ian R. Moffett, B.S.
2d Lt, USAF

Committee Membership:

Maj D. Emmons, Ph.D.
Chair

Dr. K. Obenberger, Ph.D.
Member

Dr. J. Caplinger, Ph.D.
Member

Abstract

The feasibility of using GPS data to detect fireballs is analyzed by first modeling the fireball's trail diffusion and plasma chemistry to get a resulting ion density profile of the trail over time. The signal perturbation caused by the fireball trail is simulated for a ground receiver using an analytic solution for diffraction from a Gaussian lens. Five cases were modeled with varying initial peak ion densities and altitudes taken from fireball and reentry vehicle data. This paper shows that it is feasible to detect a fireball trail using GPS if the fireball has a sufficiently high initial ion density, above approximately $10^{18}\, m^{-3}$, and occurs at an altitude above approximately 75 km. For the five cases the amplitude scintillation index, S_4, and phase scintillation index, σ_ϕ, values of the signal for the last detectable ion density profile were calculated.

Acknowledgements

I would like to thank my wife for her love, support, and patience through this journey we are taking together. I would also like to thank my thesis advisor, Maj Dan Emmons for guiding me through this journey by being a great teacher and mentor.

Ian R. Moffett

Table of Contents

Page

List of Figures

List of Tables

I. Introduction

Everyday millions of meteors enter Earth's atmosphere (1). Most are less than a millimeter in diameter, however some can range from tens of centimeters to meters in diameter. These larger meteors are called fireballs. When a meteor falls though the atmosphere it leaves a trail of ionized plasma behind it. Other than optical observations, the standard practice for detecting meteors is by using radar, which is reflecting radio waves off either the body or the plasma trail of the meteor and listening to the reflected echoes (1). The downside to this detection method is that one must have a radio transmitter and receiver near the geographic location of the meteors, and more importantly, the transmitter receiver pair must be operating during the event. This study seeks to determine if it is feasible to use the Global Positioning System (GPS) signals measured by the ground stations to detect fireballs, the advantage being total global coverage as well as constant GPS transmission.

Previous research has used GPS data to investigate ionospheric disturbances caused by explosive meteors called bolides by calculating the change in ionospheric total electron content (TEC) as a wave that propagates away from the bolide impact (2; 3), but no study has tried to directly detect fireballs using amplitude and phase data from GPS. Other studies, however, have used GPS amplitude and phase data to investigate similar ionospheric disturbances like those seen in sporadic-E (4; 5). Sporadic-E is a thin strong disturbance similar to what a fireball would produce. In (6) GPS Radio occultation (GPS-RO) is used as the signal receiver geometry. Though GPS-RO was not used in this study, techniques used to simulate and and analyze sporadic-E found in (7; 8; 9) were used as inspiration for this study to apply these techniques to fireball detection.

To determine feasibility, first a model of the fireball trail's ion density profile and its subsequent interaction with the atmosphere was made, including diffusion and

plasma chemistry. The resulting ion density profile and radius of the trail was used to perturb a simulated GPS signal traveling through the fireball trail to a GPS ground station. The diffracted signal received at the ground was then analyzed to determine if either the amplitude and/or the phase of the received GPS signal is detectable above the noise floor.

Chapter II contains the background information needed to understand the problem, methods, discussion and conclusions for someone relatively familiar to ionospheric science. Chapter III contains the methods used to model both the ion density profile of the fireball trail at various altitudes with various starting conditions as well as the methods used to model the Gaussian lens that perturbs the GPS signal. There will also be a detailed explanation of the considerations used to model the interactions between the fireball trail and the ionosphere, the methods that simulate and perturb the GPS signal, and a discussion of the results. Chapter IV will contain a brief summary of the problem, methods, and results, as well as a determination of validity and future considerations.

II. Background

2.1 Meteors

A meteor is an object made of stone and/or various metals that originated from outer space that has entered Earth's atmosphere (10). The most common type of meteor is made of stone called a chondrite (11). H-chondrites are characterized by high iron content (12) and will be approximately the type of meteor simulated in this paper. Meteors come in many different sizes but most are very small. The vast majority have a median radius of 100 μm (13). Visible meteors have a radius greater than 0.01 mm. Meteors with a radius greater than about 20 cm are called fireballs. Fireballs that explode in the atmosphere are called bolides (11). This study analyzes meteors the size of fireballs that are on the order of meters in radius.

Meteors enter Earth's atmosphere at hypersonic speeds ranging between 11–72 $km\ s^{-1}$ (11). At these extreme speeds, friction between the meteor and the atmosphere causes the surface of the meteor to heat up to thousands of Kelvin. At 2200 K the meteor will start to glow, evaporate, and ablate the surface of the meteor. The ablation of the meteor body deposits metallic ions into the surrounding atmosphere. The high temperatures during entry also cause ionization of the surrounding atmosphere. This deposition and ionization combine to form a highly ionized plasma trail behind the meteor (1). The strength and size of the plasma trail is highly dependent on the size, speed, and composition of the meteor.

The most common non-visual technique for detecting meteors utilizes the high ionization around the body and in the trail of the meteor. Using radar, radio waves will reflect off the highly ionized atmosphere and ablated material around the meteor body and trail. The reflected radio wave then travels back down to a radio receiver allowing for characterization. Some major downsides to this detection method is that

one must have a radio transmitter and receiver near the meteor's geographic location and more importantly, the transmitter receiver pair must be operating during the event (11).

2.2 Ionosphere Interactions

The ionosphere is a region of Earth's atmosphere between approximately 50 km to 1000 km characterized by elevated levels of ions (14). For this paper the altitudes of focus will be below 90 km because above 90 km electric and magnetic effects need to be taken into account. When large amounts of ions are deposited or created by the fireball, there are two major interactions that affect the ion density, namely diffusion and chemical interactions (11). Diffusion is the process by which atoms and molecules spread out over time due to factors such as collisions and gradations. Diffusion in this study comes in two forms, ambipolar diffusion of ions, and diffusion of neutrals. Chemical interactions also come in two forms, ionization and conversion. There is a multitude of interactions that can cause an ion to become a neutral or a neutral to become an ion. The specific interactions used in this paper can be found in Chapter III.

When the ionized fireball trail initially starts to diffuse, it is at its highest ion density thus the chemistry term will have the strongest effect on ion elimination. However, over time as the peak ion density decreases the diffusion terms take over as the dominating factor in ion elimination. This can be seen in Figure 1, where an example of peak loss rates from all sources can be seen changing over time.

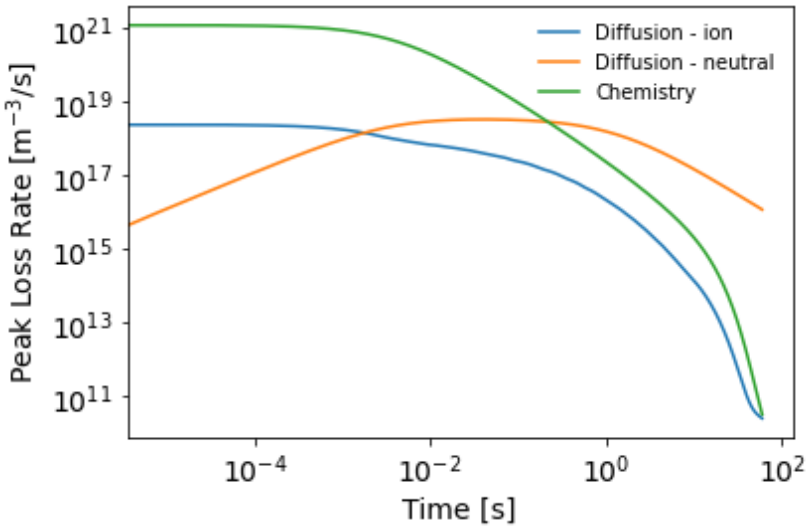

Figure 1. Peak loss rate of ion density in a fireball trail as a function of time. The green curve is the combined chemistry loss rate. The blue curve is the loss rate from ion diffusion. The orange curve shows the loss rate due to neutral diffusion.

2.3 GPS

The Global Positioning System (GPS) is a constellation of 31 satellites orbiting Earth at an altitude of approximately 20,200 km (15). GPS satellites provide a global coverage of Earth's surface, meaning that anywhere a GPS ground receiver is placed on Earth, a GPS satellite will have line of sight to the receiver. GPS satellites are also always transmitting. This means GPS helps eliminate the two biggest downsides to the radio echo method for detecting fireballs: coverage and being operational during an event. Possible downsides to using GPS to detect fireballs are availability and sensitivity. A GPS signal must propagate through the fireball trail for the signal to be perturbed. Thus, a great test bed to maximize the possibility of signal trail crossing is Japan's GEONET project which has 1,240 GPS receivers placed throughout the country (16), solving the availability issue. A distribution map of Japan's GEONET is displayed in Figure 2. In this study all simulations are preformed using conditions over Japan.

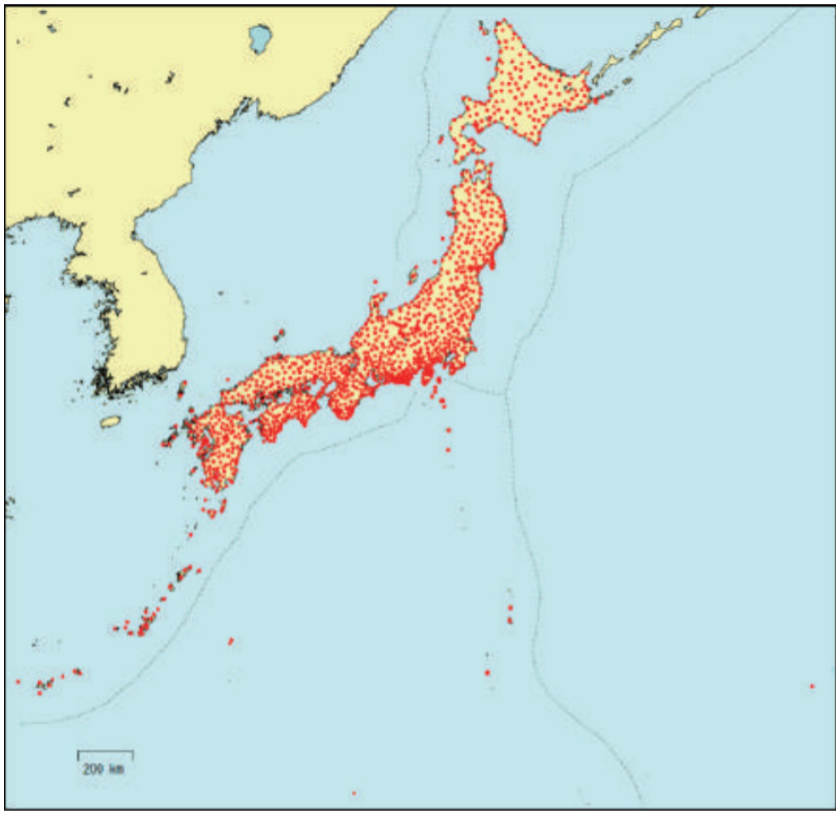

Figure 2. Map of Japan showing the geographic locations of the 1,240 GPS receivers in GEONET using red dots (Image courtesy of GIS (16)).

The second issue for using GPS to detect fireballs is timing. Figure 3 shows the geometry to consider when calculating the amount of time the GPS signal will be in the fireball trail. The time the GPS signal is in the fireball trail depends on the radius and altitude of the trail. Knowing the speed and altitude of GPS the time of trail crossing can be calculated using similar triangles. In most cases considered in this study the time to cross the trail is approximately 0.5 s to 3.5 s. Therefore, the GPS receiver must operate at an acquisition rate fast enough to capture the signal. Modern-day receivers can operate at around 100 Hz, sufficiently fast for these trail cross times, however many legacy receivers like those used for GEONET operate at 1 Hz.

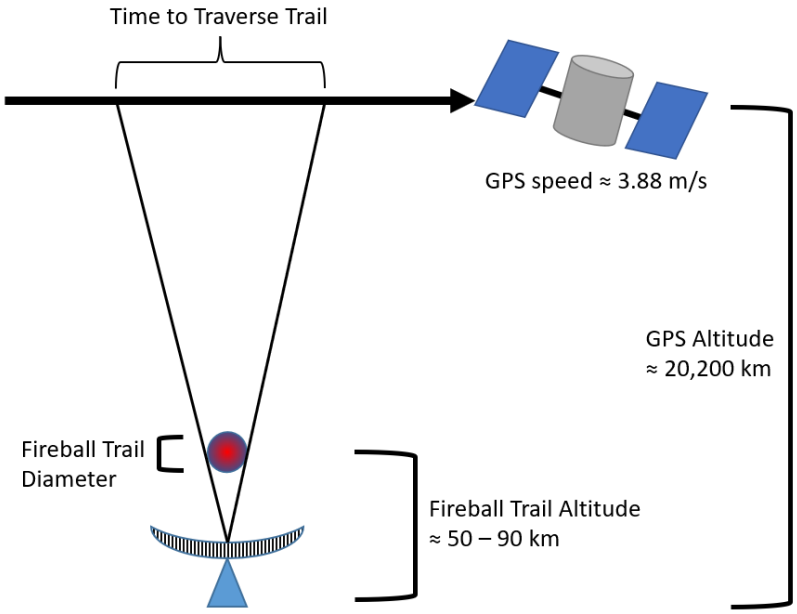

Figure 3. A simple diagram of GPS signal crossing through a fireball trail.

2.4 Plasma Lens

When the ion density of a region of the ionosphere is either higher or lower than the surrounding area, radio waves travailing through that region will be perturbed. A change in ion density changes the index of refraction. Depending on whether the change in density is positive or negative the region of differing density will act as either a positive or negative lens. In the case of a fireball trail increasing ion density relative to the surrounding area, the trail effectively becomes a negative lens. GPS is very far above the fireball trail, so by the time the GPS signal reaches the trail the signal is effectively a plane wave. When a plane wave travels through the fireball trail the signal will diffract. Depending on the strength and radius of the lens the diffraction pattern might be distinct enough to see in the received signal (17). This paper assumes that the lens formed by the fireball trail will take the form of a Gaussian profile in space. The Fresnel-Kirchhoff Integral describes the electric field as a function of x, perpendicular to the signal's direction of travel, and at an altitude

z after passing through a Gaussian lens:

$$E(X,Z) = e^{ikx}\sqrt{\frac{k}{2\pi i x}}\int_{-\infty}^{\infty}\exp\left\{\frac{ikz'^2}{2x}\right\}E(z-z',0)\,dz', \tag{1}$$

where k is the wave number. The phase of the signal after passing through the fireball trail at the ground, a distance z, can be found by taking $\phi = tan^{-1}(E_{imaginary}/E_{real})$ and the signal's intensity is $I = |E|^2$. The intensity and phase are given as a function of ground spread in kilometers. Complete ground spread detection relies on the satellite passing over the ground receiver, effectively scanning the entire signal by sliding the signal over the receiver. Figure 4 shows a GPS satellite passing over a receiver at different times. The part of the signal directly above the receiver is what is detected. Figure 4a shows the first signal that the receiver sees after the GPS's plane wave signal is perturbed by the fireball trail. As the GPS satellite flies over the receiver, the signal that the receiver detects changes as displayed in Figure 4b. The end of the detectable GPS signal is displayed in Figure 4c and by this time the receiver has seen the entire perturbed signal. The resulting signal can be stitched together to form a single signal. The length of this resulting signal is the ground spread.

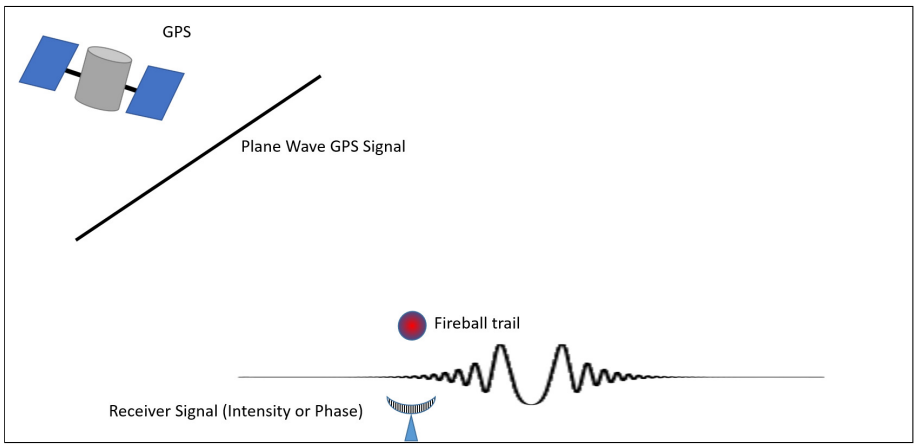

(a)

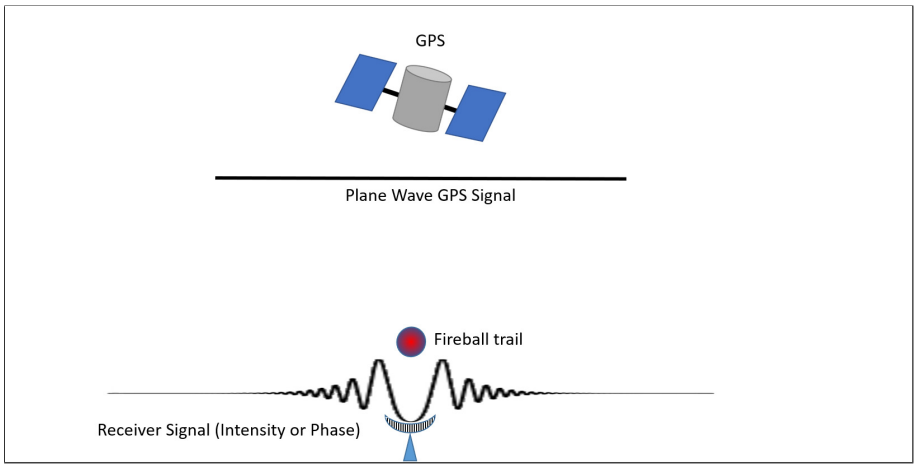

(b)

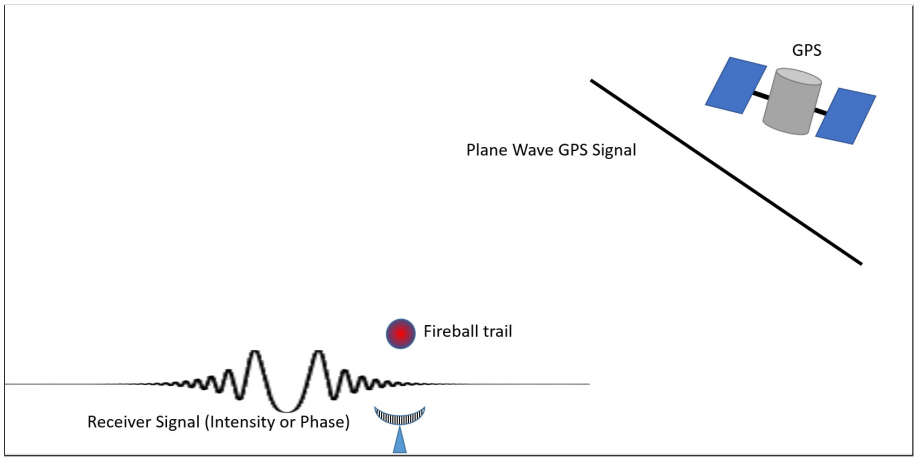

(c)

Figure 4. GPS signal seen by ground receiver over the flight path of the GPS satellite. (a) beginning of GPS satellite flight path (b) intermediate flight path (c) end of flight path.

To analyze the intensity and phase of the diffracted signal two metrics are used. First, is S_4:

$$S_4 = \sqrt{\frac{\langle I^2 \rangle - \langle I \rangle^2}{\langle I \rangle^2}}, \tag{2}$$

which is commonly known as the amplitude scintillation index. S_4 ranges from 0 to 1 for weak scatter. The noise floor for S_4 in the quiescent ionosphere is about 0.1 (18), whereas a value of S_4 greater than 0.3 is considered a significant ionospheric event and will very likely show in the data. Second, is the standard deviation of the phase, σ_ϕ. The noise floor for σ_ϕ is 0.03 rad (19). It is important to note that in this paper the standard deviation and mean are both rolling calculations with a window of 1 km because the ground spread for all cases are on the order of ones of kilometers.

III. Methodology and Results

3.1 Methods

3.1.1 Ion Density Profile.

When a fireball passes through the ionosphere it is assumed that the ablated iron and surrounding atmosphere are completely ionized. There are many interactions that a newly ionized region can have with the surrounding ionosphere. Two of the most influential interactions for ion loss are diffusion and chemical recombination. To model the ion loss, first the ionization profile of the fireball trail must be determined. The initial one-dimensional ion density profile for the fireball trail used in this model is a Gaussian of the form,

$$n_i = (n_0 - n_{bg}) \exp\left\{ \frac{-x^2}{2\sigma_r^2} \right\} + n_{bg}, \tag{3}$$

Where n_i in m^{-3} is the initial ion density as a function of position x in m along the width of the meteor trail, n_0 in m^{-3} is the initial peak ion density, n_{bg} in m^{-3} is the background ion density obtained from the International Reference Ionosphere (IRI) (20), and $\sigma_r = 2\,m$ is the initial trail radius. A σ_r of $2\,m$ comes from (11) where the initial trail radius is approximately twice the initial fireball radius. For this paper the initial fireball radius is chosen to be $1\,m$ as a typical fireball size. An example of the initial ion density profile of a simulated fireball trail is displayed in Figure 5.

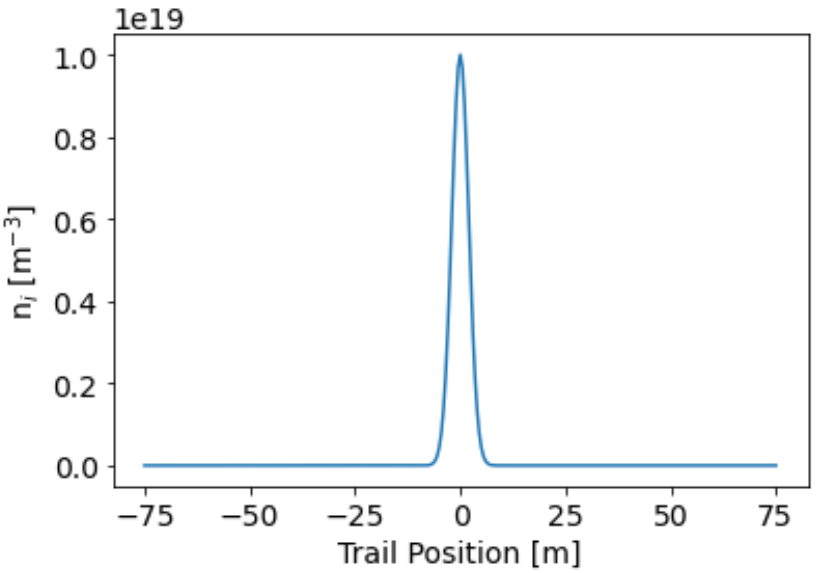

Figure 5. An example of the initial ion density profile for a simulated fireball. n_i **in** m^{-3} **is the ion density of the fireball trail along the trails x-axis 1-D cross section. Trail position in** m **is along the x-axis, perpendicular to the meteor's direction of travel and spans the width of the simulated cross section, -75** m **to 75** m**, in this case. The initial model parameters for this example are:** $n_0 = 10^{19}\, m^{-3}$**,** $n_{bg} = 4 \times 10^8\, m^{-3}$**, and** $\sigma_r = 2\, m$**.**

After the initial ion density profile for the fireball trail is determined, diffusion and recombination can be simulated. First the chemical recombination is calculated. The simulated fireball is assumed to be mostly made of iron (12), thus Fe^+ is the dominate ion and via quasi-neutrality, $Fe^+ \approx n_e$. The rate at which the ion density n decreases over time is the rate of Fe^+ production made from iron neutral (Fe) minus the rate of iron neutral production made from Fe^+ (recombination rate). This combined rate R_c is given by:

$$R_c = R_{Fe^+} - R_{Fe}, \tag{4}$$

where R_{Fe^+} is the production rate of Fe^+ given by,

$$R_{Fe^+} = [Fe](k_8[O_2^+] + k_9[NO^+] + k_{10}), \tag{5}$$

and R_{Fe} is loss rate of Fe^+ and is given by

$$R_{Fe} = [Fe^+][n_i]\Bigg[\left(k_1[O_3] + (k_2[O_2][M] + k_3[N_2][M])\frac{k_4[O]}{k_4[O] + k_7[n_i]}\right)\frac{k_6}{k_6[n_i] + k_5[O]} + (k_2[O_2][M] + k_3[N_2][M])\frac{k_7}{k_4[O] + k_7[n_i]} + k_{11} + k_{3ee}[n_i] + k_{3A}[M]\Bigg]. \tag{6}$$

Here, $[n_i]$ is the quasi-neutral ion (electron) density, in this case $[n_i] \approx [Fe^+]$, $[M]$ is the concentration of the dominate neutral molecule, in all cases for this model $M = N_2$, and rate coefficients k_1–k_{11}, k_{3ee}, and k_{3A} can be found in Table 1.

Table 1. Rate coefficients for Equation 5 and Equation 6. Rates k_1–k_{11} are from (21), rates k_{3ee}, the three-body electron-electron, and k_{3A}, the three body electron-neutral, are from (22) and (23) respectively.

Rate coefficient	Reaction	Rate coefficient value	Units
k_1	$Fe^+ + O_3 \rightarrow FeO^+ + O_2$	$7.6 \times 10^{-10} \exp\{-241/T\}$	$cm^3 s^{-1}$
k_2	$Fe^+ + O_2 + M \rightarrow FeO_2^+ + M$	$1.7 \times 10^{-29}(T/300)^{-1.83}$	$cm^6 s^{-1}$
k_3	$Fe^+ + N_2 + M \rightarrow FeN_2^+ + M$	$8.0 \times 10^{-30}(T/300)^{-1.52}$	$cm^6 s^{-1}$
k_4	$FeO_2^+, FeN_2^+ + O \rightarrow FeO^+ + O_2, N_2$	1×10^{-10}	$cm^3 s^{-1}$
k_5	$FeO^+ + O \rightarrow Fe^+ + O_2$	7×10^{-12}	$cm^3 s^{-1}$
k_6	$FeO^+ + e^- \rightarrow Fe + O$	$1 \times 10^{-7}(200/T)^{0.5}$	$cm^3 s^{-1}$
k_7	$FeO_2^+, FeN_2^+ + e^- \rightarrow Fe + O_2, N_2$	$3 \times 10^{-7}(200/T)^{0.5}$	$cm^3 s^{-1}$
k_8	$Fe + O_2^+ \rightarrow Fe^+ + O_2$	1.1×10^{-9}	$cm^3 s^{-1}$
k_9	$Fe + NO^+ \rightarrow Fe^+ + NO$	9.2×10^{-10}	$cm^3 s^{-1}$
k_{10}	$Fe + h\nu \rightarrow Fe^+ + e^-$	5×10^{-7}	s^{-1}
k_{11}	$Fe^+ + e^- \rightarrow Fe + h\nu$	1×10^{-12}	$cm^3 s^{-1}$
k_{3ee}	$Fe^+ + e^- + e^- \rightarrow Fe + e^-$	1×10^{-24}	$cm^6 s^{-1}$
k_{3A}	$Fe^+ + e^- + M \rightarrow Fe + M$	1×10^{-26}	$cm^6 s^{-1}$

Using an explicit finite difference method with forward difference for time and central difference for space (FTCS), the iron ion and iron neutral density can be

calculated below,

$$\frac{[Fe^+]_j^{k+1} - [Fe^+]_j^k}{\Delta t} = D_i \frac{[Fe^+]_{j+1}^k - 2[Fe^+]_j^k + [Fe^+]_{j-1}^k}{\Delta x^2} + R_{c,j}^k, \tag{7}$$

and,

$$\frac{[Fe]_j^{k+1} - [Fe]_j^k}{\Delta t} = D_n \frac{[Fe]_{j+1}^k - 2[Fe]_j^k + [Fe]_{j-1}^k}{\Delta x^2} - R_{c,j}^k \tag{8}$$

where k is the temporal index, j is the spatial index, R_c is the chemical rate from Equation 4, D_i and D_n are the ion and neutral diffusion rates respectively, Δt is the current time step in the simulation, and Δx is the differential length along the density profile. It is important to keep track of both the iron ion density from Equation 7 (the final output of the trail model) and the neutral density in Equation 8 because the chemical rate equations, Equation 5 and Equation 6 use $[Fe^+]$ and $[Fe]$, which change over time.

The ion and neutral diffusion coefficients D_i, and D_n, can be calculated using the following process laid out in (24):

$$\begin{aligned}
D_i &= \frac{2k_b T_e}{m_{Fe}\nu_{ni}}, \\
D_n &= \frac{k_b T_n}{m_{Fe}\nu_{nn}}, \\
\nu_{nx} &= n_{N_2}\sigma_{nx}v_{nx}, \\
\sigma_{nx} &= \pi(r_x + r_{N_2})^2, \\
v_{nx} &= \sqrt{\frac{8k_b T_x}{\pi\mu}}, \\
\mu &= \frac{m_{Fe}m_{N_2}}{m_{Fe} + m_{N_2}},
\end{aligned} \tag{9}$$

In Equation 9 the subscript x is either i or n referring to Fe^+ and Fe respectively. ν_{nx} is the average collision frequency in $1/s$, σ_{nx} is the solid sphere collisional cross

section in m^2, v_{nx} is the average relative speed in m/s, and μ is the reduced mass in kg. The values for unchanging constants in Equation 9 can be found in Table 2. In this model the most prevalent neutral molecule is N_2, thus N_2's parameters are built into Equation 9. It should be noted that in Equation 9, the iron ion collisional

Table 2. Constants used to determine the ion diffusion coefficients in Equation 9. Values for the constants were obtained from National Institute of Standards and Technology (NIST)

Constant	Value	Units
k_b	1.38×10^{-23}	J/K
m_{Fe}	9.27×10^{-26}	kg
m_{N_2}	4.65×10^{-26}	kg
r_{Fe}	140×10^{-12}	m
r_{N_2}	364×10^{-12}	m

frequency ν_{ni} is not calculated via Equation 9. This is because the hard sphere cross-section is no longer a valid assumption when dealing with ions because the hard sphere doesn't take into count the polarization and electric effects. ν_{ni} is instead equal to $\nu_{ni} = 3.5 \times 10^{16}\, m^3 s^{-1} \times n_{N2}$ (25).

For time marching, every time t to t_{end}, Fe and Fe^+ are solved at every grid point along the profile in increments of Δt. At $t = 0$, the ion density is at it's maximum, thus the loss rates are at a maximum as well. This requires a smaller Δt at the beginning when sensitivity is crucial for increased accuracy. Subsequently over time, as the peak ion density and loss rates decrease a larger Δt can be used so save computation time. To determine the appropriate value for Δt at any given time, Δt is solved for after every step using the Courant–Friedrichs–Lewy condition (CFL) (26). The CFL states that Δt must be sufficiently small such that the distance travel in Δt is smaller than the step size taken in the spatial dimension. The CFL used here is

$$\Delta t_{CFL} = \frac{0.5 \Delta x^2}{D}, \tag{10}$$

where D is the largest diffusion coefficient. However, the CLF only accounts for diffusion excluding any chemical contributions. If the chemical ion loss rate is high, a large Δt can cause an overshoot when using the finite difference method, thus decreasing accuracy. So, a sufficiently small Δt needs to be calculated such that the fractional decrease in peak ion density is controlled. Solving for Δt via chemistry contribution is as follows:

$$\Delta t_{chem} = \frac{1 \times 10^{-3} n_{peak}}{R_{c_1 peak}}, \tag{11}$$

where 1×10^{-3} is the fraction of the peak ion density to reduce for at each time step, n_{peak} is the current peak ion density, and $R_{c_1 peak}$ is the peak loss rate from only chemical contributions. Finally, the Δt used at a given time step is the smaller of Δt_{CFL} or Δt_{Chem}, thus always satisfying the CFL condition while accounting for rapid chemical ion loss. Using a time loop, one can find the final ion density profile, $[Fe^{+}(x)]$, at any given time. This final ion density profile is then used as the Gaussian lens to perturb a GPS signal.

3.1.2 Gaussian lens.

Using the ion density profile, the strength of the Gaussian lens, ϕ_0, can be calculated. The plasma frequency profile, $f_p(x)$, follows

$$\begin{aligned} f_p &= \frac{1}{2\pi}\sqrt{\frac{e^2 n_e}{m_e \epsilon_0}}, \\ f_p &\approx 8.98\sqrt{n_e}, \end{aligned} \tag{12}$$

where f_p is the plasma frequency in Hz, e is the elementary charge of the electron, n_e is the electron density (ion density via quasi-neutrality) in m^{-3}, m_e is the mass of the electron, and ϵ_0 is the permittivity of free space (14). Then, the index of refraction

profile, $\eta_p(x)$, is calculated using

$$\eta_p = \sqrt{1 - \frac{f_p^2}{f_{signal}^2}} \tag{13}$$

where f_{signal} is the frequency of the signal passing through the meteor trail, in this case GPS's L1 band ($f_{signal} = 1575.42\ MHz$). Next, the difference in index of refraction from the background refractive index, η_{bg}, is calculated:

$$\Delta\eta(x) = \eta_p(x) - \eta_{bg}. \tag{14}$$

Next, the strength of the lens is,

$$\phi_0 = k_{L1} \int_{-x_t}^{x_t} \Delta\eta(x)\, dx, \tag{15}$$

where k_{L1} is the wave number ($2\pi/\lambda_{L1}$) of the GPS L1 frequency and the bounds of the integral cover the entire trail cross section. Lastly, from the ion density profile obtained from diffusion and chemistry calculations, the trail radius r_0, in m is the half width at $1/e$ from maximum.

For the Gaussian lens made by a fireball trail with radius r_0 the complex electric field at the ground after the GPS signal passes through the lens can be found by taking a power series of Equation 1 as outlined in (17) to obtain

$$E(X, Z) = \sum_{n=0}^{\infty} \frac{(i\phi_0)^n}{n!} (1 + 2niX)^{-1/2} \exp\left\{ -\frac{nZ^2}{1 + 2niX} \right\}, \tag{16}$$

where X is

$$X = \frac{x}{kr_0^2}, \tag{17}$$

and x is the desired ground spread length and Z is

$$Z = \frac{z}{r_0}, \tag{18}$$

where z is the altitude of the fireball trail. By truncating Equation 16 after 100 terms, a very close approximation to the true electric field can be quickly found by a computer. Finally, the phase of the signal after passing through the meteor trail at the ground, a distance z, can be found by taking $\phi = tan^{-1}(E_{imaginary}/E_{real})$ and the signal's intensity is $I = |E|^2$.

3.2 Results

The simulation outlined in the previous section was performed for five different scenarios, four of which are based on real measured events while one is a theoretical ideal scenario for maximal detection. Of the four measured events, three are of reentry vehicles (Stardust, Apollo capsule, and Ram-C), the remaining one is of a fireball. Due to the rarity of large meteors entering Earth's atmosphere as well as detection issues outlined in Chapter II, measurements of ion densities in large meteor trails are rare. In lieu of meteor measurements, reentry vehicle measurements were used. The reentry vehicle measurements take place at typical fireball altitudes and produce ion densities similar to fireballs, making them good proxy measurements. Table 3 contains the measured ion densities and altitudes for each scenario including the theoretical ideal scenario for detection. The ion densities in Table 3 are used as the initial peak ion densities for the model.

Each of the five scenarios occur at different altitudes as shown in Table 3. For each altitude various parameters pertaining to the model change. Table 4 contains all the altitude dependent variables. The background temperature and ion densities were

Table 3. For the five different simulated events each sources ion density in m^{-3}, and altitude in km are shown. The three reentry vehicle's data are from (27) and the fireball data is from (28).

Source	Peak Ion Density (m^{-3})	Altitude (km)
Fireball	1×10^{19}	50
Ram-C	1×10^{18}	60
Apollo Capsule	3×10^{20}	75
Stardust	2×10^{20}	81
Ideal	1×10^{19}	90

obtained from IRI. The neutral densities were obtained from the Mass Spectrometer Incoherent Scatter model (MSIS), (29) except for O_3, which was taken from (30). Both IRI and MSIS were run at local midnight over Japan at latitude 37° and longitude of 140°. Local midnight was selected because it has low surrounding ion density compared to local noon (14).

Table 4. Initial input parameters for the meteor model at each altitude. Neutral concentrations were obtained from MSIS and temperature and ion concentrations were obtained from IRI. Both MSIS and IRI were run at local midnight at latitude of 37° and longitude of 140°.

Altitude (km)	Temperature (K)	N_2 (m^{-3}) $\times10^{19}$	O_2 (m^{-3}) $\times10^{19}$	O (m^{-3}) $\times10^{15}$	O_3 (m^{-3}) $\times10^{14}$	O_2^+ (m^{-3}) % n_e	NO^+ (m^{-3}) % n_e	n_e (m^{-3}) $\times10^{7}$
90	179.7	5.169	1.320	178.5	8.5	0.5	99.5	49.38
81	190.1	30.88	8.188	4.292	8.0	0	100	0.302
75	200.6	68.63	18.30	0.144	7.5	0	0	0
60	241.7	289.5	149.2	0	6.0	0	0	0
50	262.8	1920	515.0	0	5.0	0	0	0

While discussing the upcoming five scenarios, the term detection or detectable level is determined by the lens strength and radius combination producing either a detectable (above the noise floor) $S_4 > 0.1$ or phase standard deviation, $\sigma_\phi > 0.03$ rad after the signal passes through the trail, as measured by a ground based GPS receiver.

3.2.1 Fireball.

Using input values from Table 3 and Table 4 at 50 km, ion density profiles were calculated at various times. As displayed in Figure 6 the time to reach a small ϕ_0, the lens strength, is very quick at milliseconds. Also, the trail's radius did not increase significantly over time as the diffusion rate requires a longer time for trail radius expansion. This is due to the loss rate for chemistry (diving the peak ion density down) being many orders of magnitude stronger than the peak ion diffusion rate as displayed in Figure 7. The last detectable ϕ_0 is $\phi_0 = -3.0$ radians at a trail radius of 3.5 m.

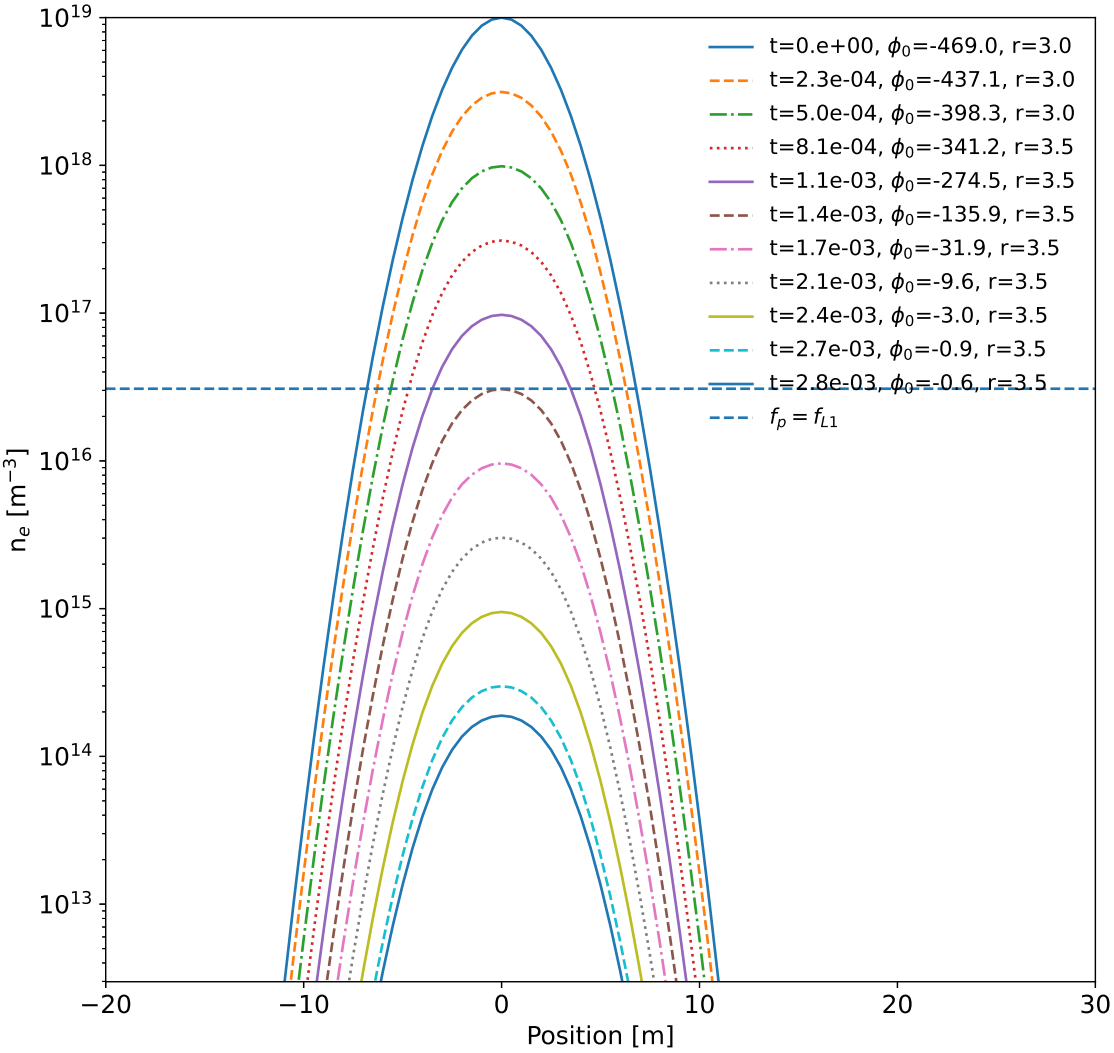

Figure 6. The ion density profile at various times. For each profile a time in seconds, lens strength ϕ_0 in radians, and a trail radius in meters is shown. The dashed line is the point at which the trail's plasma frequency is equal to GPS's L1 frequency.

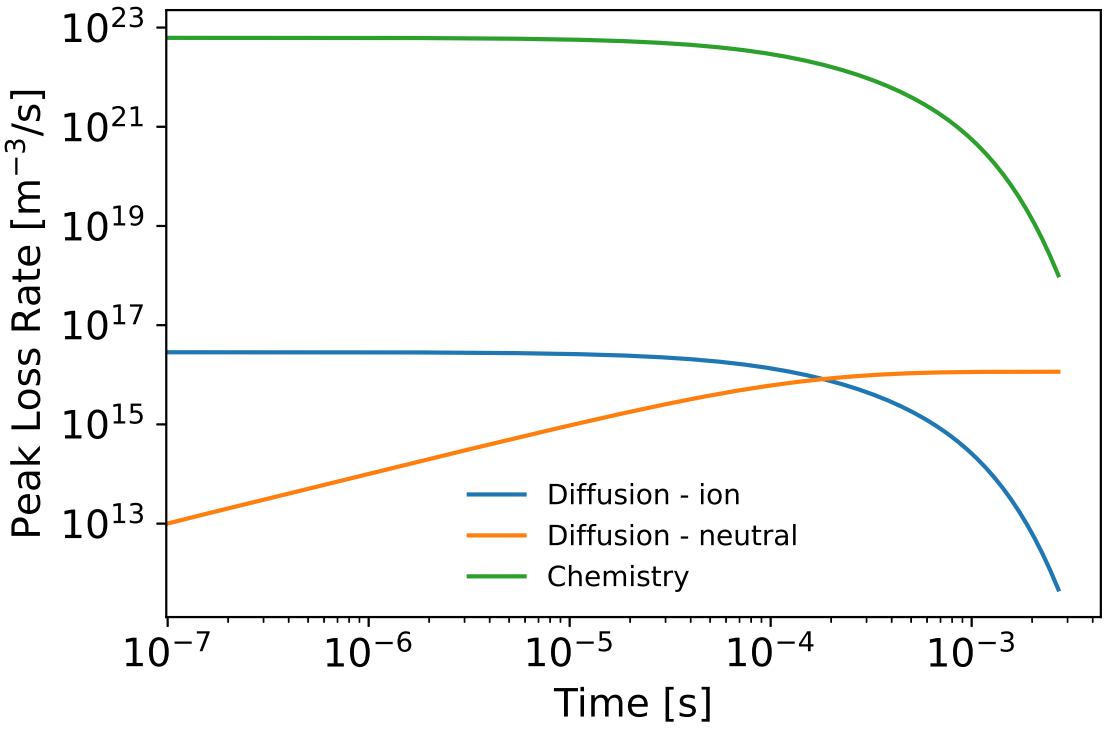

Figure 7. The peak loss rates at the last time step for the Fireball scenario. The green line is the ion loss rate due to chemistry. The blue line is the ion loss due to the diffusion of ions, and the orange line is the neutral loss rate due to the diffusion of neutrals.

Using $\phi_0 = -3.0$ rad and a trail radius of 3.5 m, the plane wave diffraction was simulated, the results of which can be found in Figures 8–11. Figure 8 shows the GPS signals normalized intensity as a function of ground spread in km.

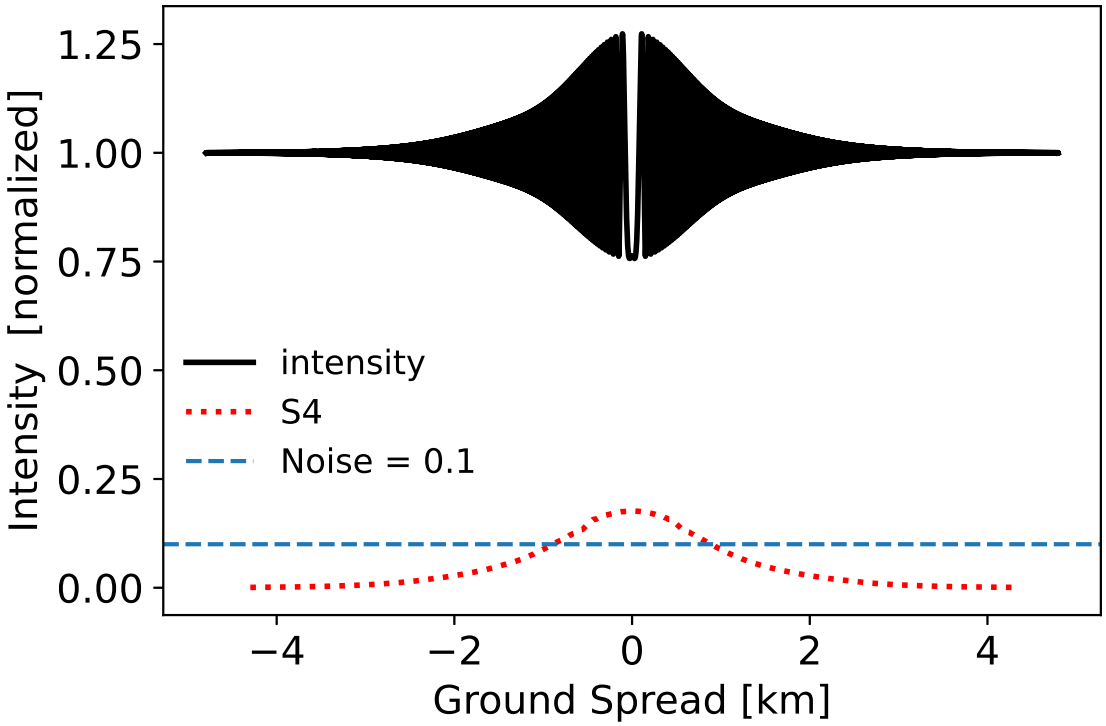

Figure 8. The resulting normalized intensity after passing through the fireball trail at an altitude of 50 km with $\phi_0 = -3.0$ rads and $r = 3.5\,m$. The blue dashed line shows the noise floor and the red dotted line shows the rolling S_4 with a window of 1 km.

Plotted on Figure 8, as a dashed blue line, is the 0.1 noise floor discussed in Chapter II. The dotted red line is the rolling S_4 calculation with a window of 1 km. Table 5 contains the important results from the four figures including the maximum S_4 value, which is above the noise floor for this scenario. Thus, the scintillation caused by this fireball scenario could be measured.

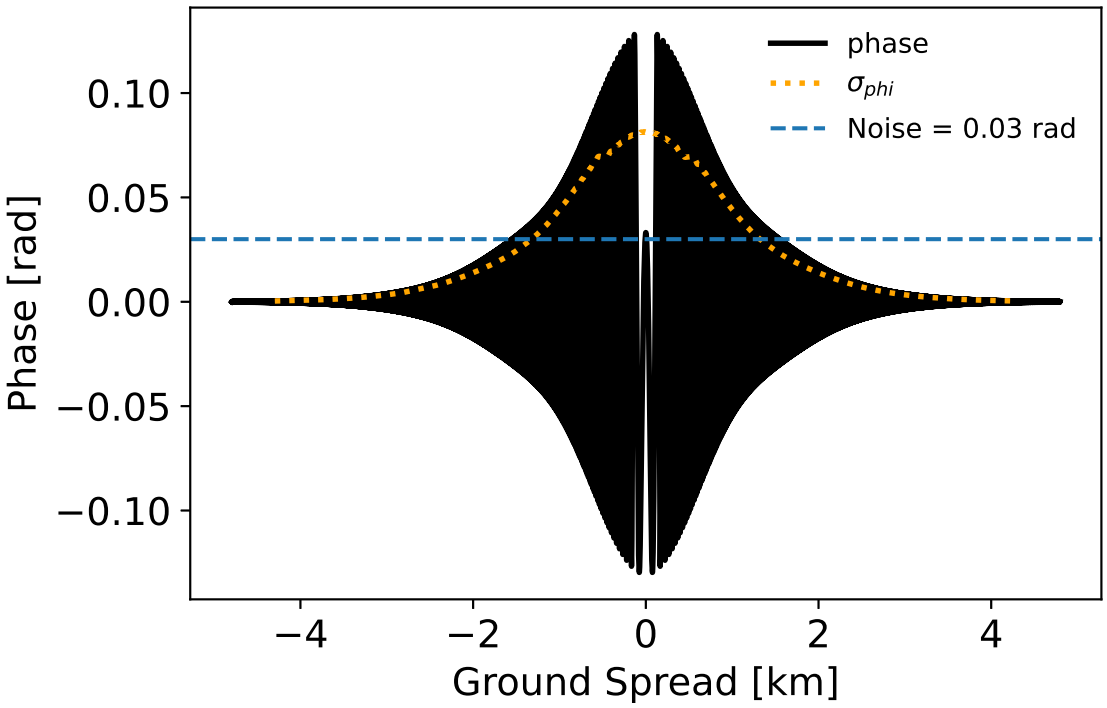

Figure 9. The resulting signal phase after passing through the fireball trail at an altitude of 50 km with $\phi_0 = -3.0$ radians and $r = 3.5\,m$. The blue dashed line shows the noise floor and the yellow dotted line shows the σ_ϕ calculated with a 1 km window.

Shown in Figure 9 and Table 5 the maximum standard deviation of the phase σ_ϕ, is also above the 0.03 rad noise floor suggesting that the phase scintillation could be measured. Figure 10 is a power spectrum of the signal intensity whose important features can be found in Table 5.

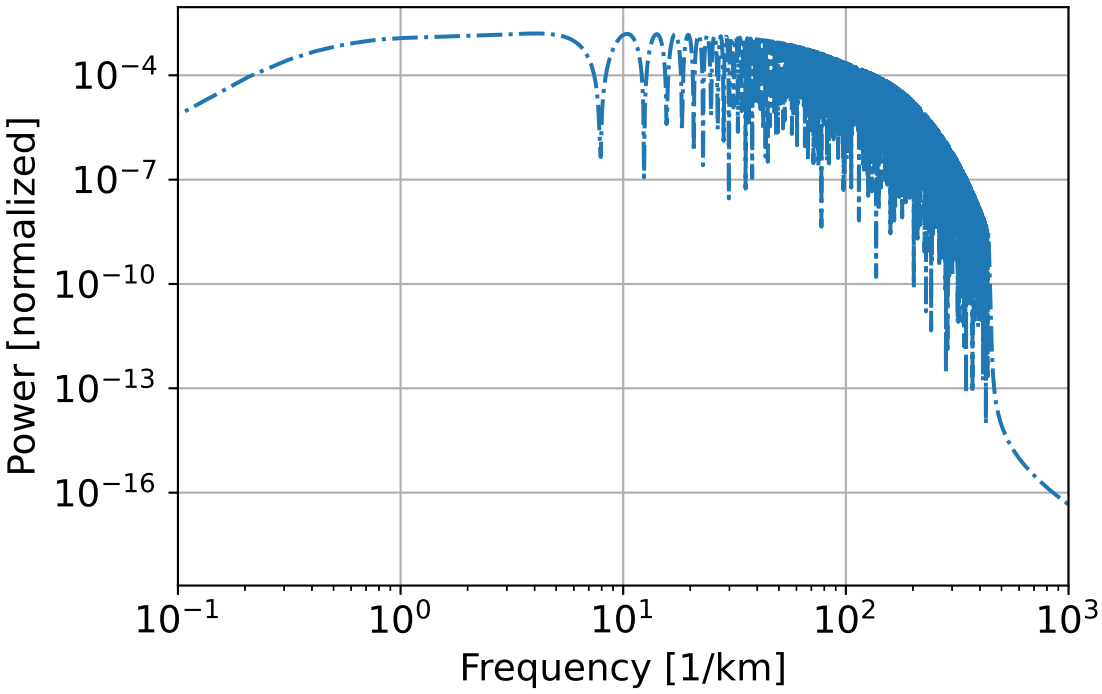

Figure 10. The power spectrum of the signal intensity after passing through the trail at an altitude of 50 km with $\phi_0 = -3.0$ rads and $r = 3.5\,m$.

Figure 11 shows the wavelet spectrogram of the intensity. Looking at the shape the wavelet makes, could help identify the fireball in the data because of the unique inverted V-shape the wavelet transform makes that would not be seen in random noise. The V-shape, or inverted V-Shape is a wavelet spectrogram is known as a chirp. The wavelet spectrogram could also be helpful in situations where the intensity S_4 is not above the noise floor as the wavelet spectrogram could reveal the a chirp in the data.

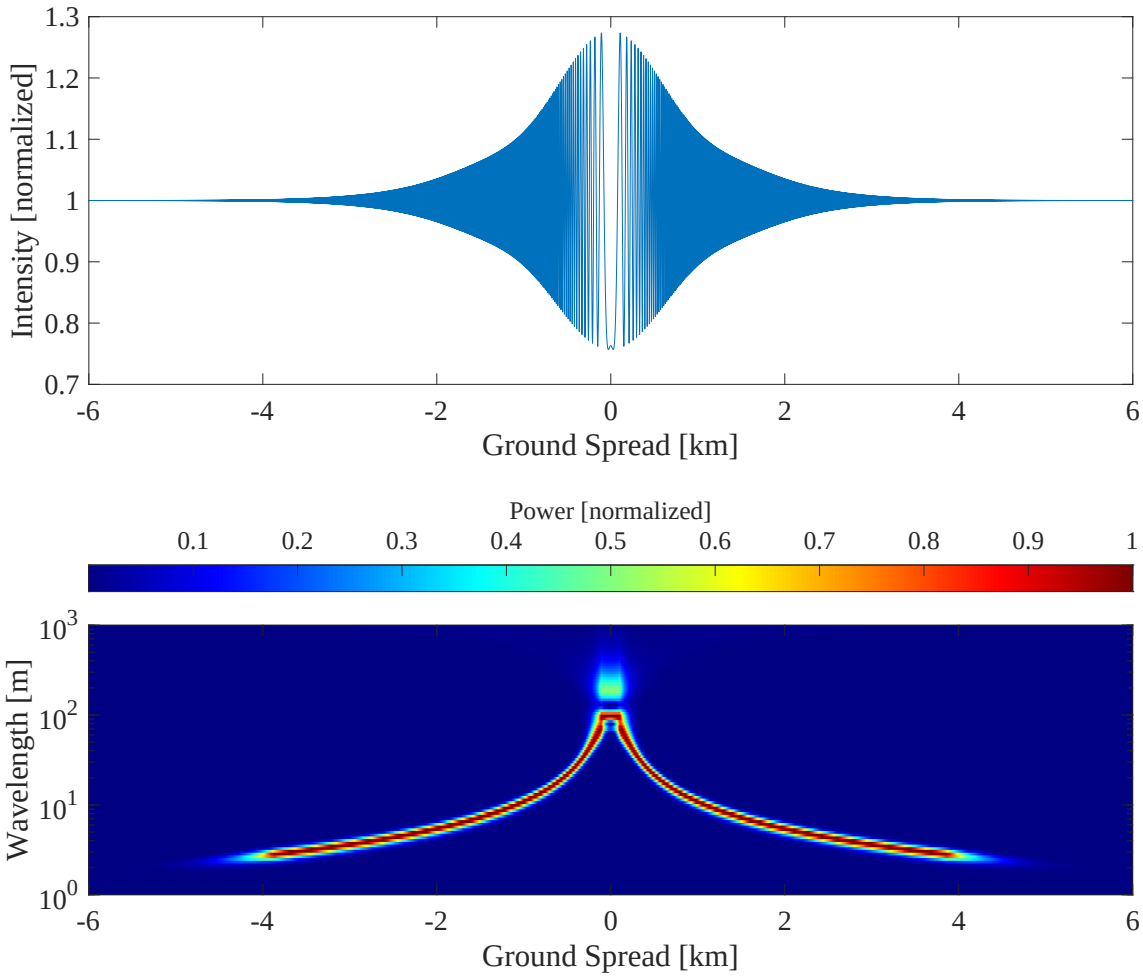

Figure 11. The wavelet spectrogram (PSD as a function of ground spread) of the signal after passing through the trail at an altitude of 50 km with $\phi_0 = -3.0$ rads and $r = 3.5m$.

Even though the instantaneous phase can be measured, the fireball will become undetectable in milliseconds. This is due to its low altitude causing very small diffusion coefficient, thus limiting the trail radius. More importantly, high concentrations of neutral species cause the iron ions to recombine rapidly, dropping the peak ion density to undetectable levels well before the GPS signal could be perturbed by the trail. To be able to detect the trail the GPS must cross the entire trail cross-section. If the trail doesn't last for at least 0.5 seconds, the GPS receiver will not be able to detect the entire ground spread as discussed in Chapter II, GPS.

Table 5. Important results for the fireball scenario with the trail at an altitude of 50 km with $\phi_0 = -3.0$ rads and $r = 3.5\,m$.

S_4 Max	= 0.18
σ_{phi} Max [rad]	= 0.08
Peak frequency [1/km]	= 4.07

3.2.2 Ram-C.

Increasing the altitude to 60 km, Ram-C's ion density profiles can be seen in Figure 12. For Ram-C the radius doesn't change during this time frame despite being at a higher altitude than the previous fireball scenario. This is because the initial ion density is low compared to the fireball's initial ion density, thus Ram-C's peak density is reduced to undetectable levels before it has the time to diffuse. Even though the total detectable time (0.038 sec) is longer for Ram-C than the fireball scenario (0.0028 sec), the time is still too quick for detection. However, if detection timing was sufficient, the lowest detectable lens strength is $\phi_0 = -1.3$ with a trail radius of 3 m. Using the previous two values, lens strength and radius, the effect of the trail on the simulated signal as measured by a ground based GPS receiver can be seen in Figure 13 and Figure 14.

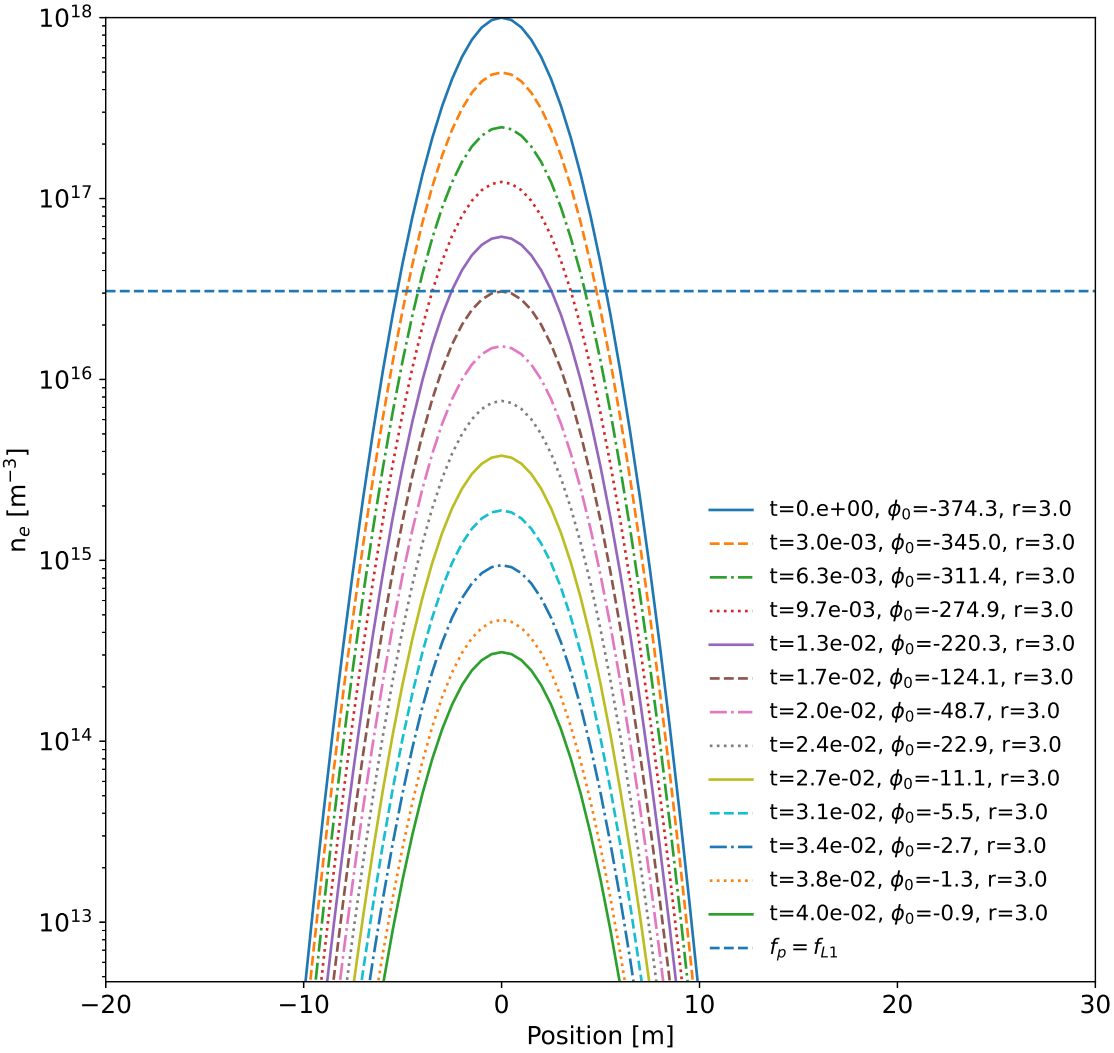

Figure 12. The ion density profile at various times. For each profile a time in seconds, lens strength ϕ_0 in radians, and a trail radius in meters is shown. The dashed line is the point at which the trail's plasma frequency is equal to GPS's L1 frequency.

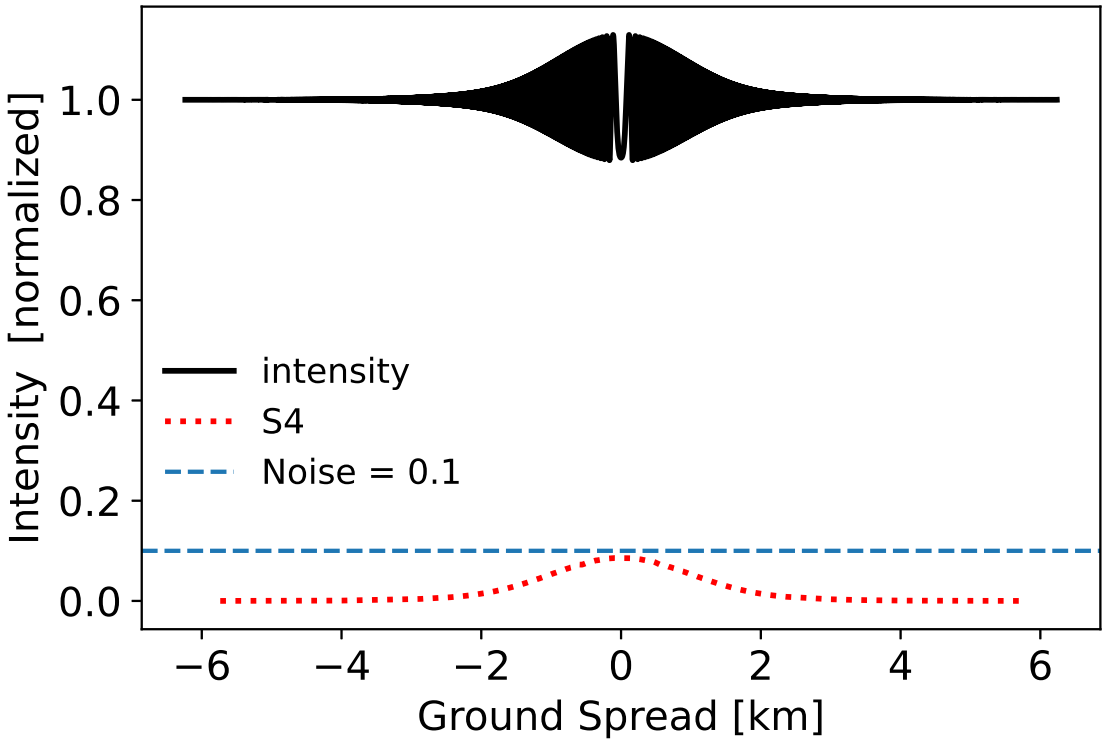

Figure 13. The resulting normalized intensity after passing through the fireball trail at an altitude of 60 km with $\phi_0 = -1.3$ rads and $r = 3\,m$. The blue dashed line shows the noise floor and the red dotted line shows the rolling S_4 with a window of 1 km.

As displayed in Table 6 Ram-C's maximum S_4 is not over the noise floor of 0.1. This is likely because the peak ion density at the last detectable time is low enough to cause a low lens strength. At $t = 3.4 \times 10^{-2}$ sec, $\phi_0 = -2.7$ rads, and $r = 3$ m, Ram-C's S_4 maximum is 0.13, which is above the noise floor. However, at the last detect time, Ram-C's maximum S_4 is not over the noise floor of 0.1 but, σ_ϕ displayed in Figure 14 is over the noise floor and could be detected. Figure 15 is a power spectrum of the signal and Figure 16 shows the wavelets. Their important features can be found in Table 6.

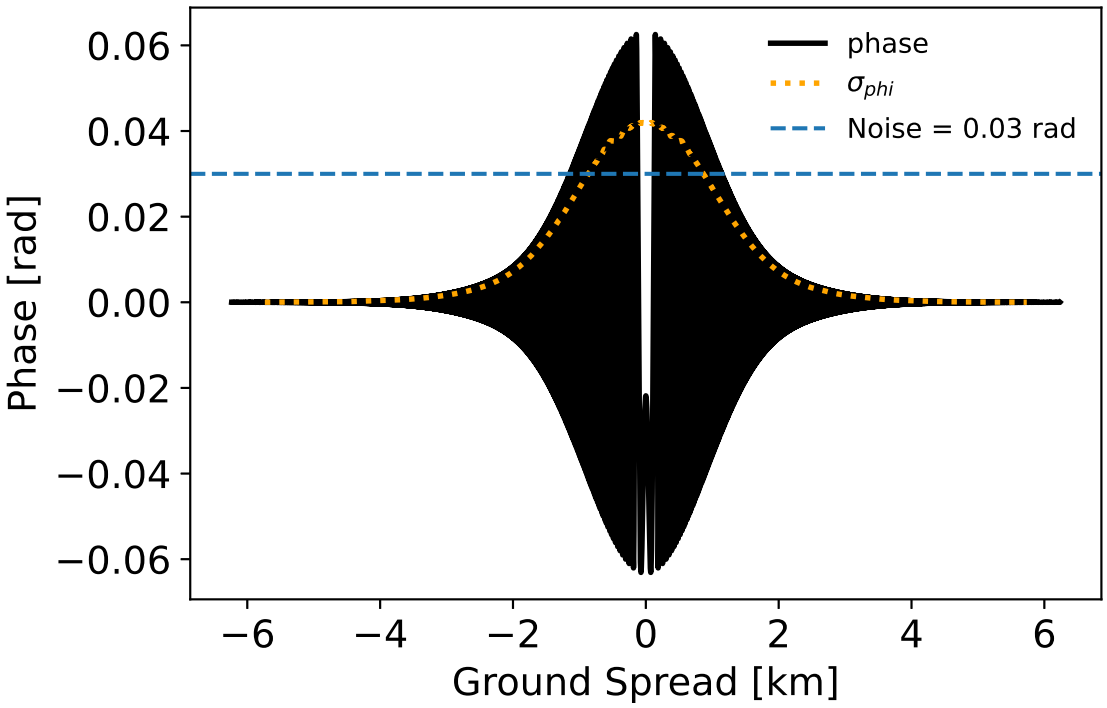

Figure 14. The resulting signal phase after passing through the fireball trail at an altitude of 60 km with $\phi_0 = -1.3$ rads and $r = 3\,m$. The blue dashed line shows the noise floor and the yellow dotted line shows the σ_ϕ calculated with a 1 km window.

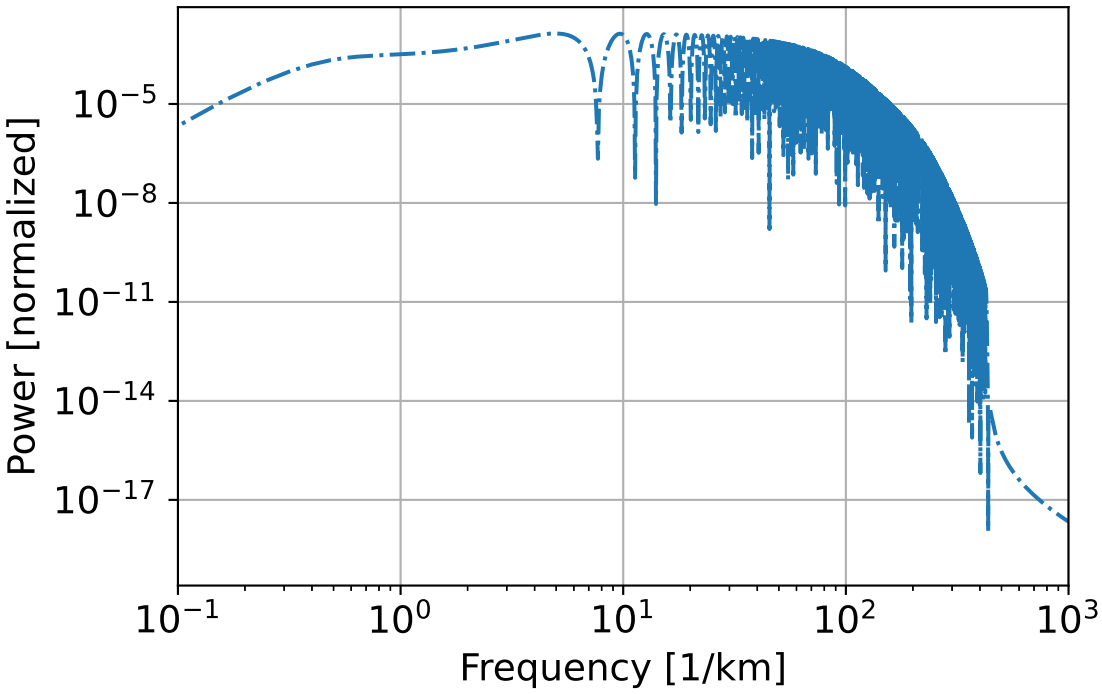

Figure 15. The power spectrum of the signal intensity after passing through the trail at an altitude of 60 km with $\phi_0 = -1.3$ rads and $r = 3\,m$.

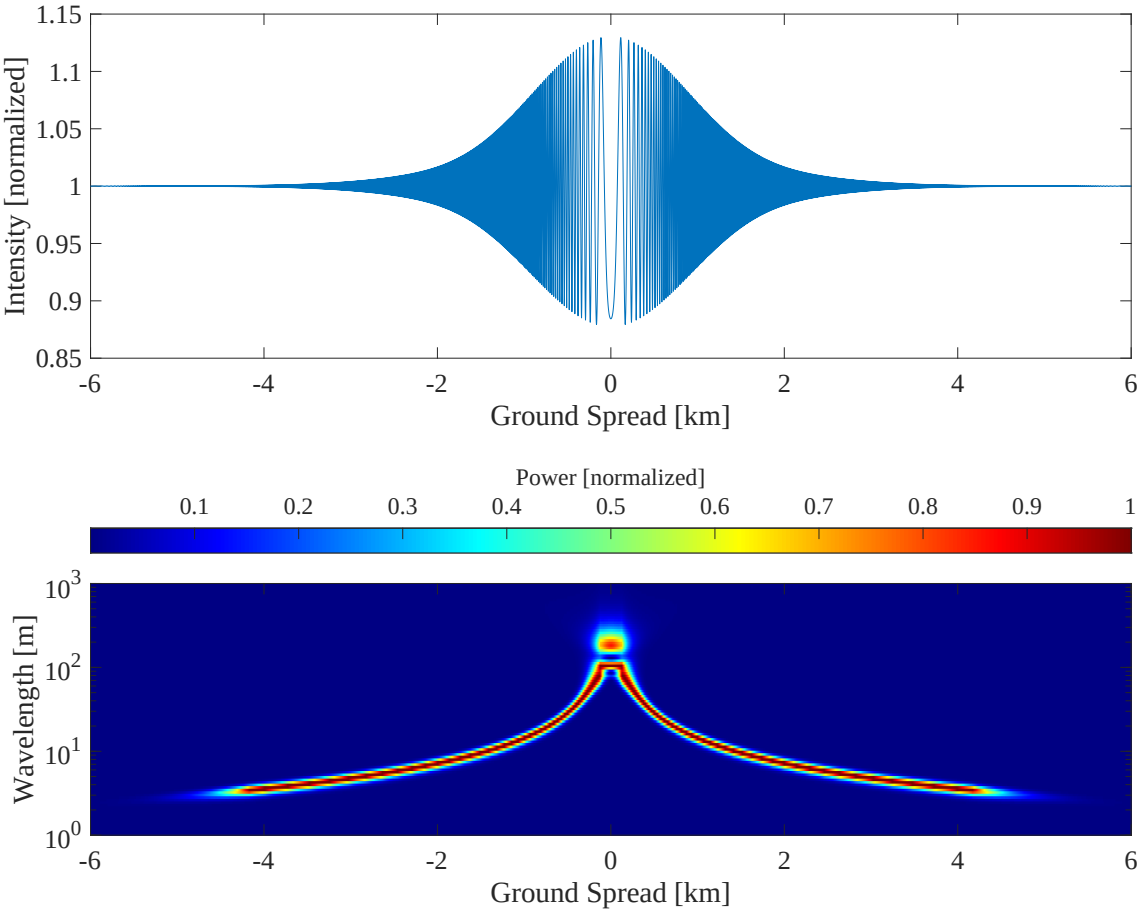

Figure 16. The wavelet spectrogram (PSD as a function of ground spread) of the signal after passing through the trail at an altitude of 60 km with $\phi_0 = -1.3$ rads and $r = 3\,m$.

Ram-C would not likely be detected, again due to a short lifetime before peak ion density is reduced to undetectable levels. Like in the fireball scenario, the problem for detection is with the low altitude causing a small diffusion coefficient, thus limiting the trail radius and high concentrations of neutral species causing the iron ions to recombine rapidly, dropping the peak ion density to undetectable levels well before the GPS signal could be perturbed by the trail.

Table 6. Important results from Ram-C's trail at an altitude of 60 km with $\phi_0 = -1.3$ rads and $r = 3\,m$.

S_4 Max	$= 0.086$
σ_{phi} Max [rad]	$= 0.042$
Peak frequency [1/km]	$= 4.971$

3.2.3 Apollo Capsule.

Increasing in altitude to 75 km, the Apollo capsule's ion density profile displayed in Figure 17 shows a longer range of time, approximately one second, compared to the previous two scenarios. With one second of elevated ion density the likelihood of signal crossing and detection from GPS is now feasible. Also, at this altitude and the longer time, diffusion is able to increase the trail radius to more than double that of the previous scenarios. The last detectable lens strength is $\phi_0 = -5.9$ rads at a trail radius of 7.5 m. Once more, using the lens strength and radius, the effect on the GPS signal can be simulated.

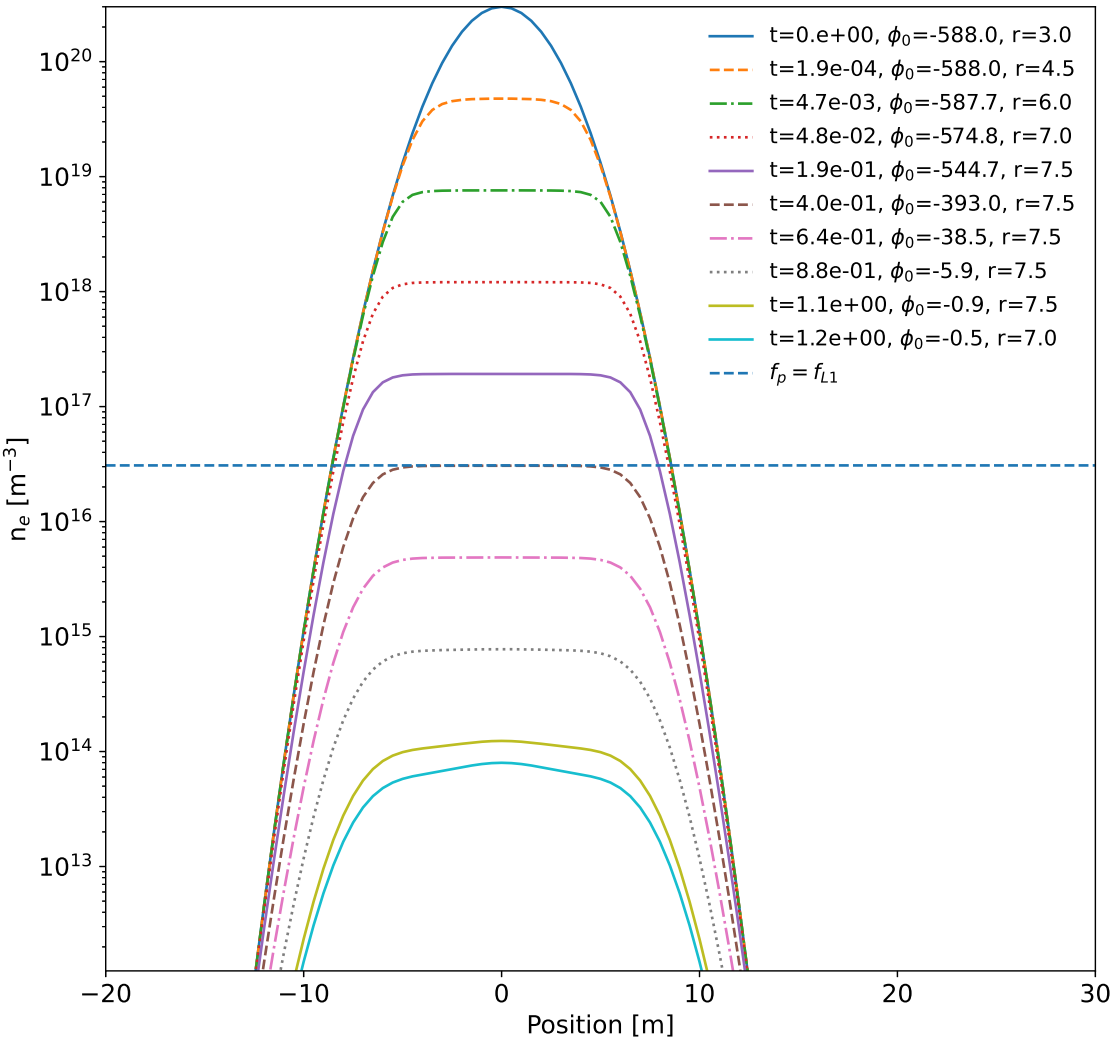

Figure 17. The ion density profile at various times. For each profile a time in seconds, lens strength ϕ_0 in radians, and a trail radius in meters is shown. The dashed line is the point at which the trail's plasma frequency is equal to GPS's L1 frequency.

Displayed in Figure 18 and Table 7, it can be seen that the Apollo capsule's S_4 is above the noise floor. Though an S_4 of 0.3 is generally considered a significant event, Apollo capsule's S_4 peak at approximately 0.211 is likely to be seen in the data.

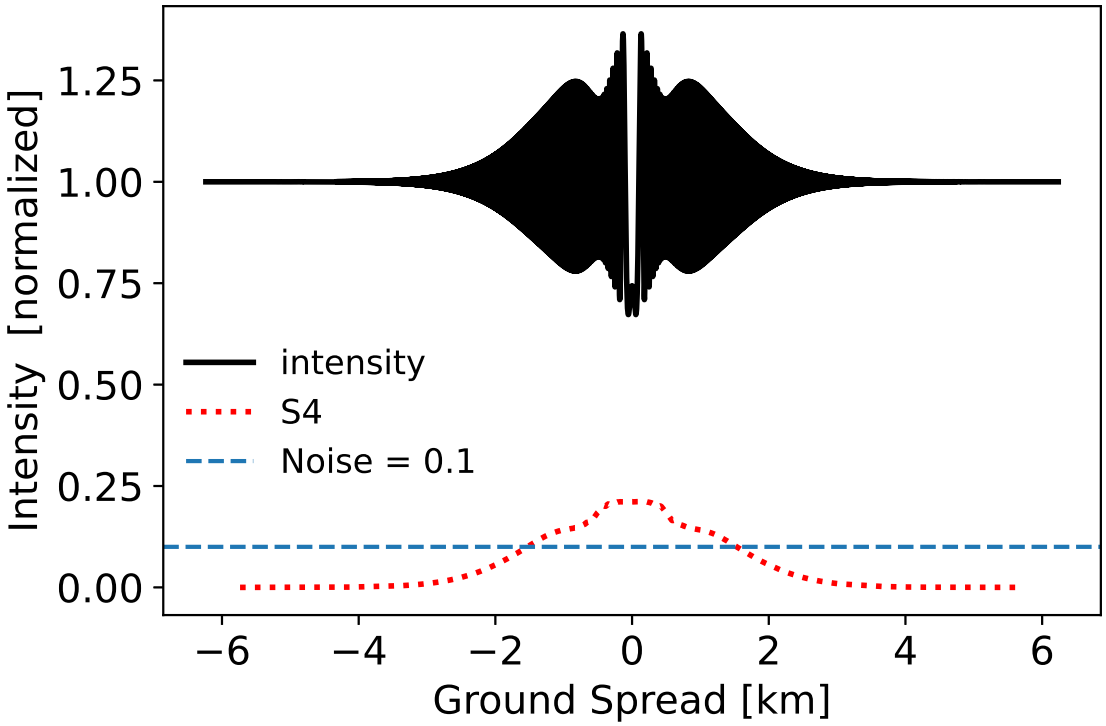

Figure 18. The resulting normalized intensity after passing through the fireball trail at an altitude of 75 km with $\phi_0 = -5.9$ rads and $r = 7.5\,m$. The blue dashed line shows the noise floor and the red dotted line shows the rolling S_4 with a window of 1 km.

Apollo's σ_ϕ is also above the noise floor and high enough that detection is likely (Figure 19 and Table 7).

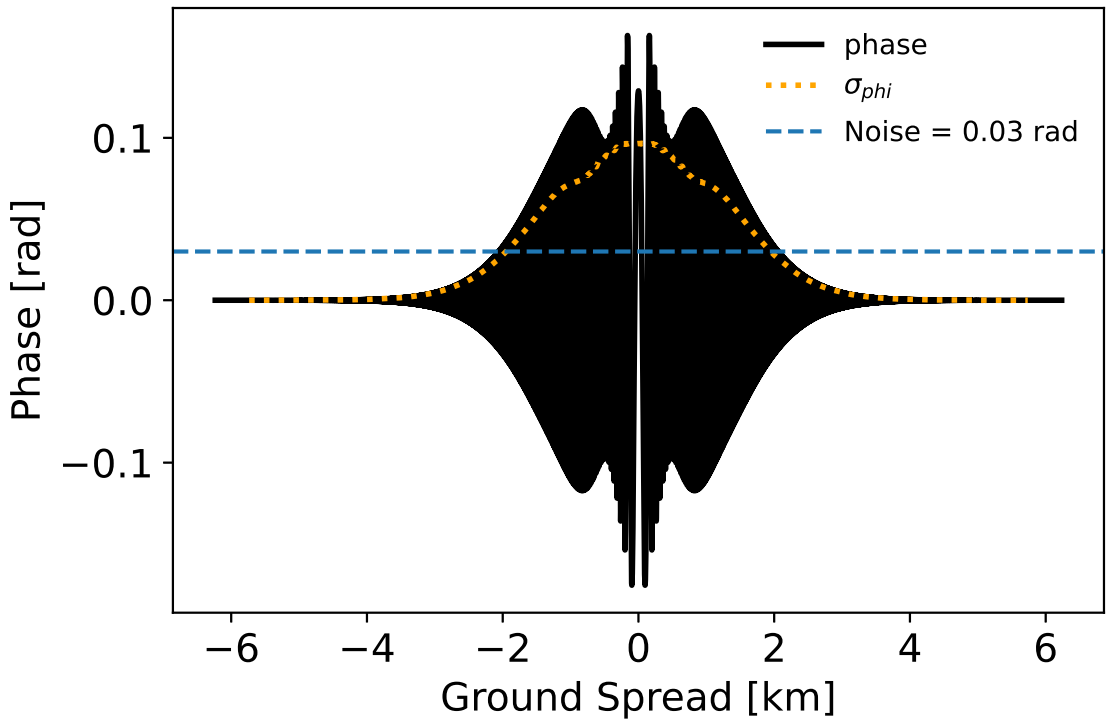

Figure 19. The resulting signal phase after passing through the fireball trail at an altitude of 75 km with $\phi_0 = -5.9$ rads and $r = 7.5\,m$. The blue dashed line shows the noise floor and the yellow dotted line shows the σ_ϕ calculated with a 1 km window.

Figure 20 is a power spectrum of the signal and Figure 21 shows the wavelets. Their important features can be found in Table 7.

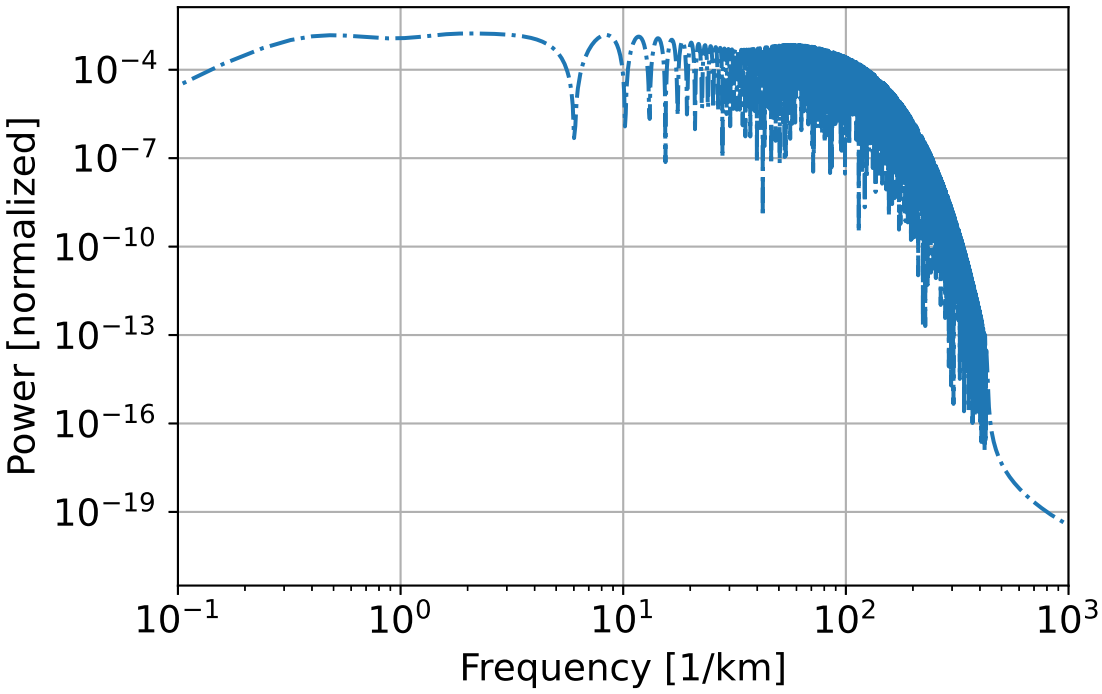

Figure 20. The power spectrum of the signal intensity after passing through the trail at an altitude of 75 km with $\phi_0 = -5.9$ rads and $r = 7.5\,m$.

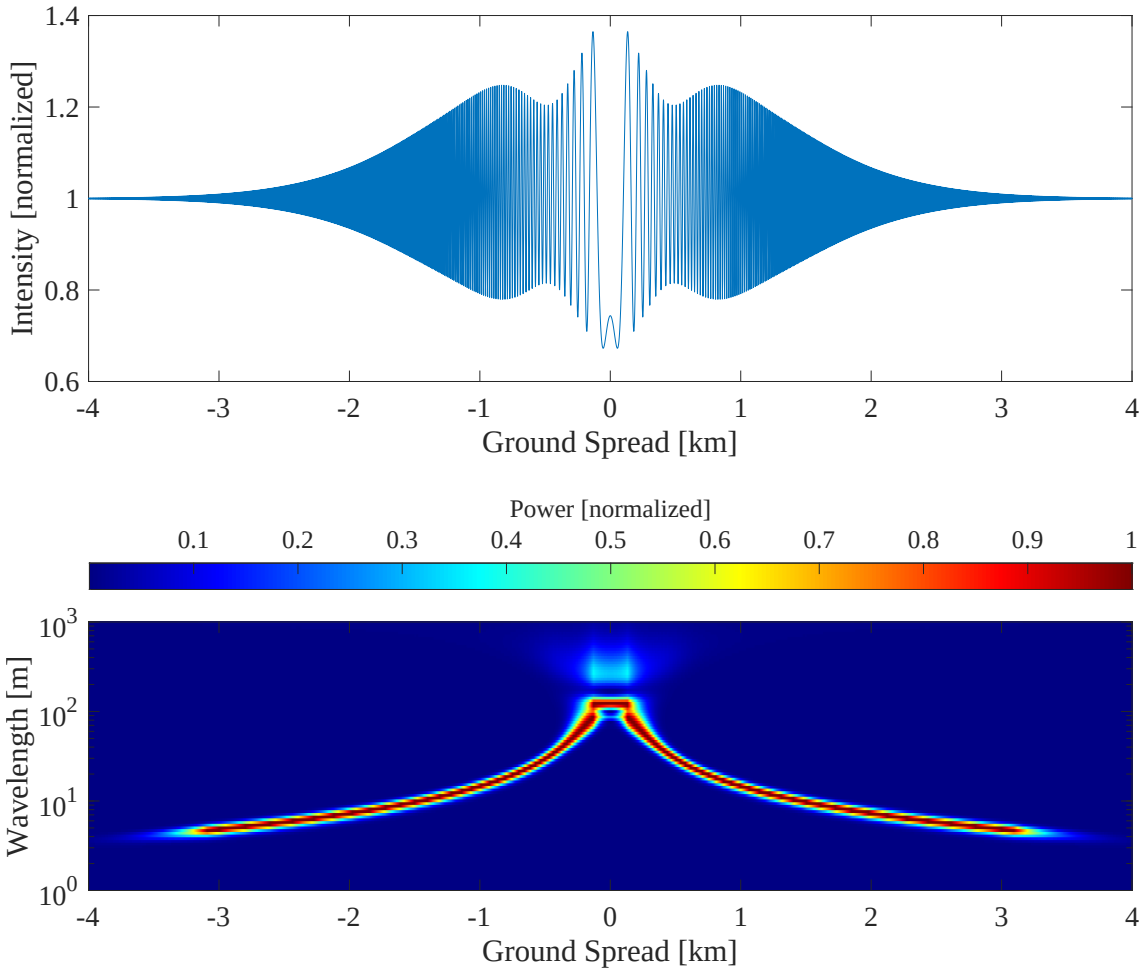

Figure 21. The wavelet spectrogram (PSD as a function of ground spread) of the signal after passing through the trail at an altitude of 75 km with $\phi_0 = -5.9$ rads and $r = 7.5m$.

Apollo is the first of the five scenarios that detection is feasible because the trail remained detectable long enough for a GPS signal to pass though trial to get an entire ground spread signal at a receiver. Apollo's high altitude and high initial ion density enabled it to last long enough for detection and for the trail's radius increase through diffusion.

Table 7. Important results from Apollo capsule's trail at an altitude of 75 km with $\phi_0 = -5.9$ rads and $r = 7.5\,m$.

S_4 Max	= 0.211
σ_{phi} Max [rad]	= 0.097
Peak frequency [1/km]	= 2.084

3.2.4 Stardust.

Stardust, with an altitude of 81 km, which is greater than the previous examples, has sufficiently high diffusion coefficients such that trail radius nearly doubles allowing significant diffusion of the trail radius. However, by the time the trail radius diffuses to large radii the lens strength dips below detection giving a final detectable radius at 7.5 m just like the Apollo capsule. The difference between Stardust and the Apollo capsule is that Stardust's trail lasts for almost five seconds before becoming undetectable. During that period it reaches a maximum trail radius of 8 m, and lens strength of -43.8 rads at 1.3 seconds.

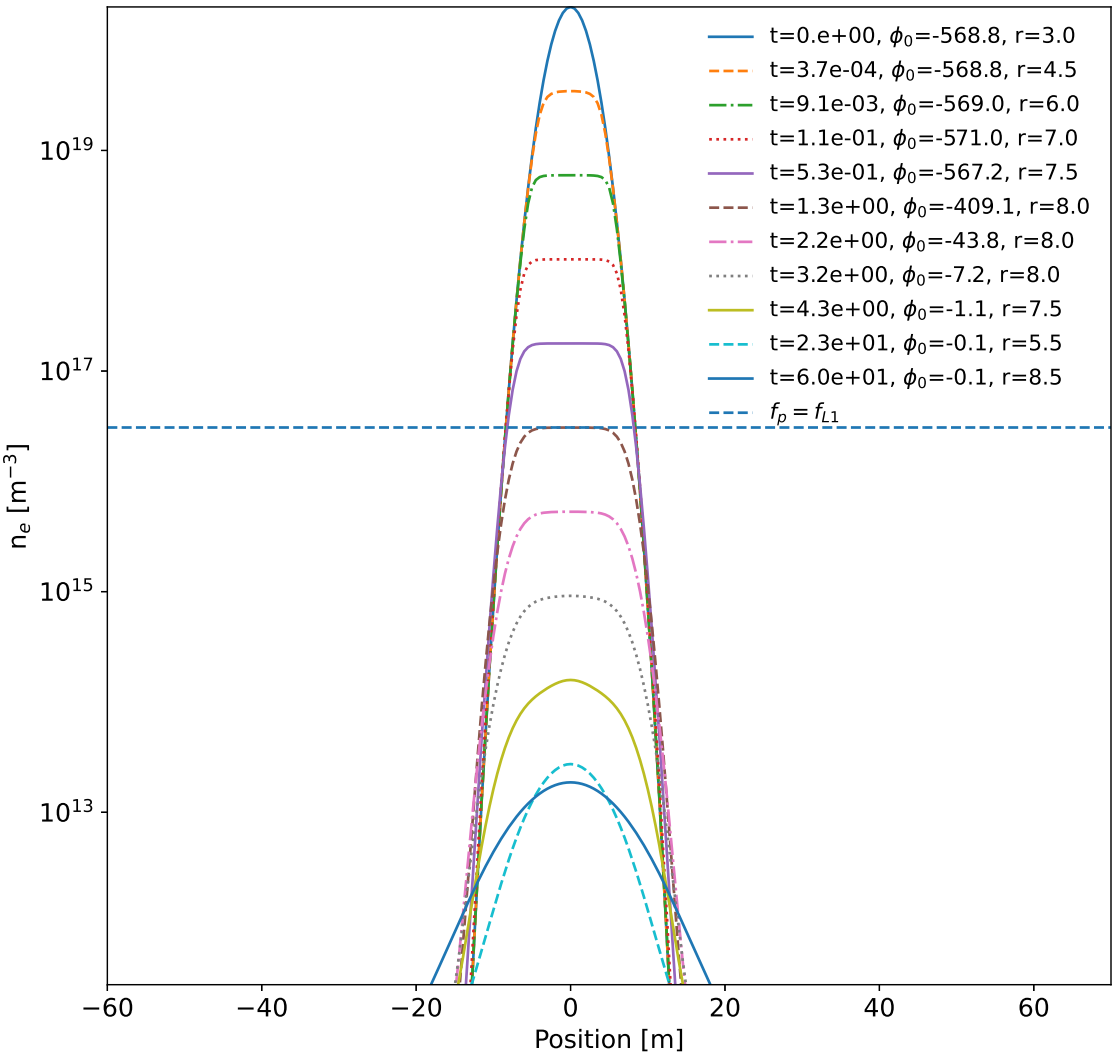

Figure 22. The ion density profile at various times. For each profile a time in seconds, lens strength ϕ_0 in radians, and a trail radius in meters is shown. The dashed line is the point at which the trail's plasma frequency is equal to GPS's L1 frequency.

Analyzing the last detectable time at 4.3 seconds, lens strength of -1.1 rads, and a trail radius of 7.5 m, Figure 23 shows the GPS signal intensity after passing through the trail. Table 8 contains the maximum S_4 value, which is only slightly above the noise floor, not strong enough for it to stand out prominently in the data. Figure 24 shows the signal phase after passing through Stardust's trail.

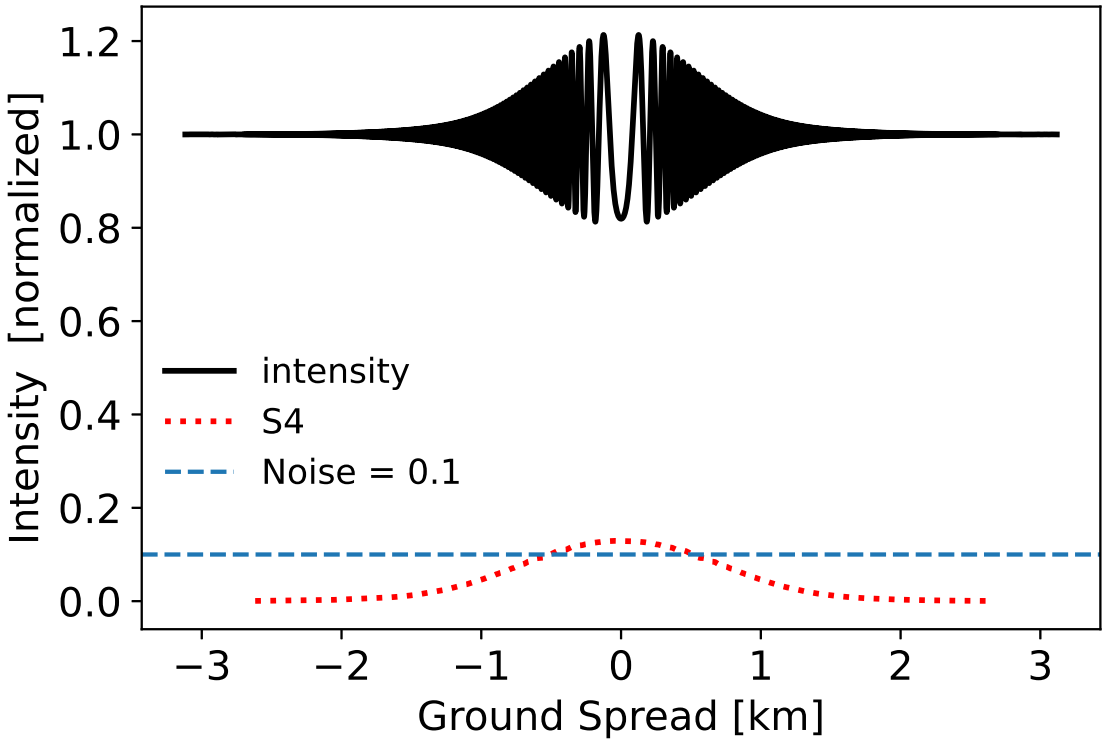

Figure 23. The resulting normalized intensity after passing through the fireball trail at an altitude of 81 km with $\phi_0 = -1.1$ rads and $r = 7.5\,m$. The blue dashed line shows the noise floor and the red dotted line shows the rolling S_4 with a window of 1 km.

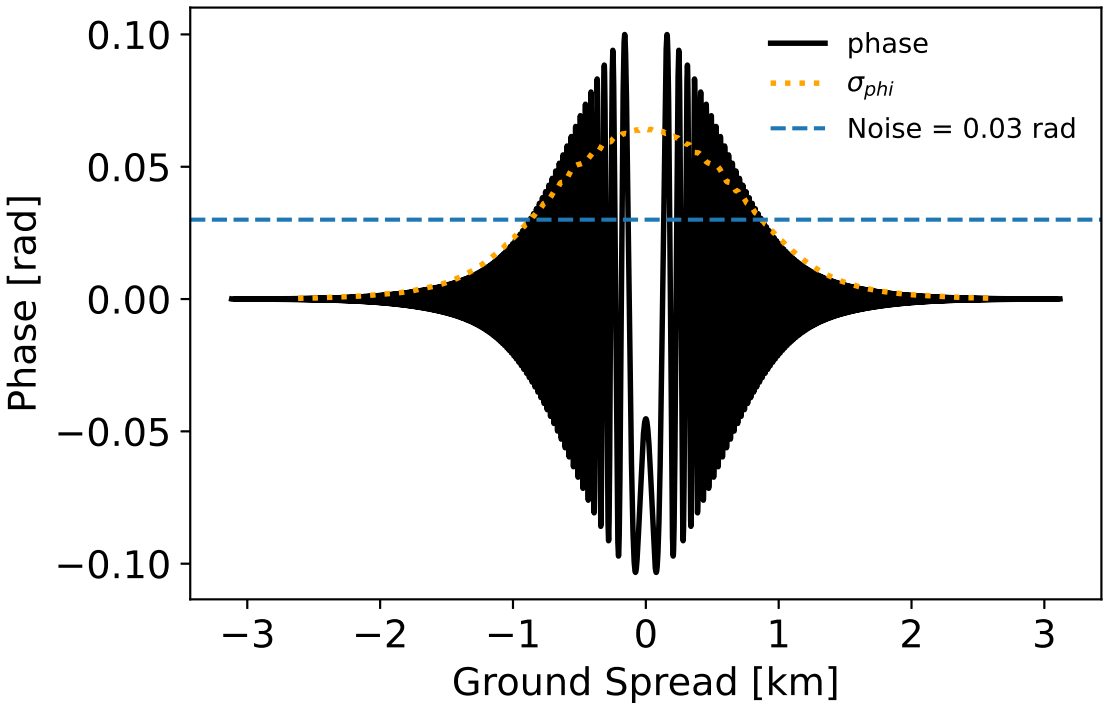

Figure 24. The resulting signal phase after passing through the fireball trail at an altitude of 81 km with $\phi_0 = -1.1$ rads and $r = 7.5\,m$. The blue dashed line shows the noise floor and the yellow dotted line shows the σ_ϕ calculated with a 1 km window.

The maximum σ_ϕ at 0.06 rad is well above the noise floor and thus has a high likelihood of showing prominently in the data.

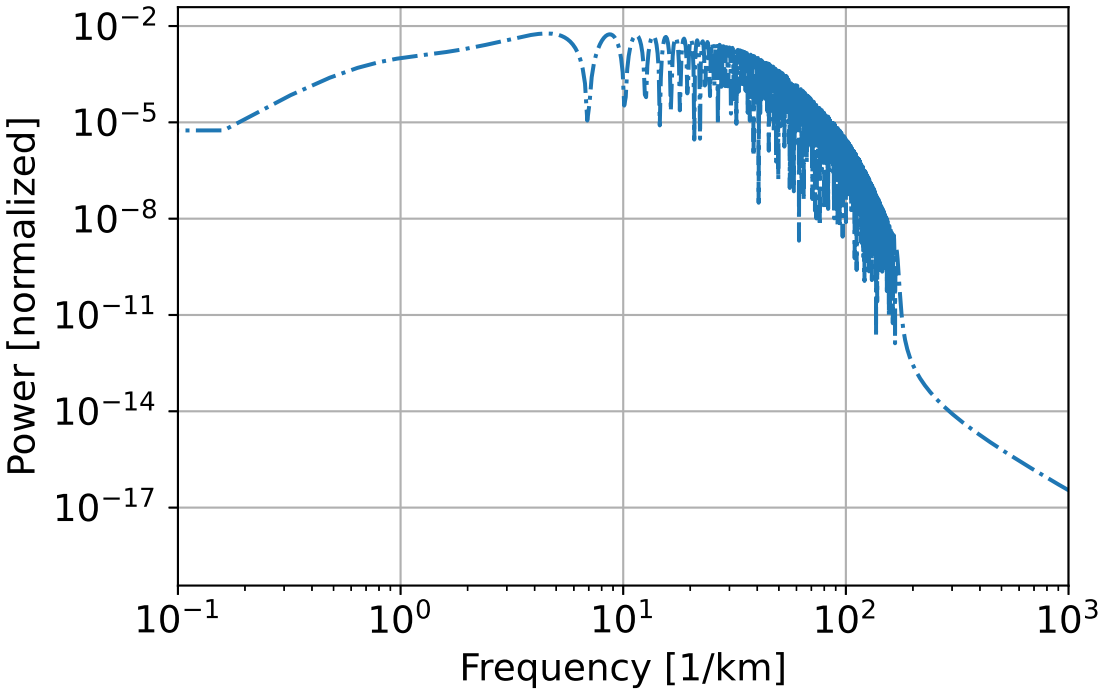

Figure 25. The power spectrum of the signal intensity after passing through the trail at an altitude of 81 km with $\phi_0 = -1.1$ rads and $r = 7.5\,m$.

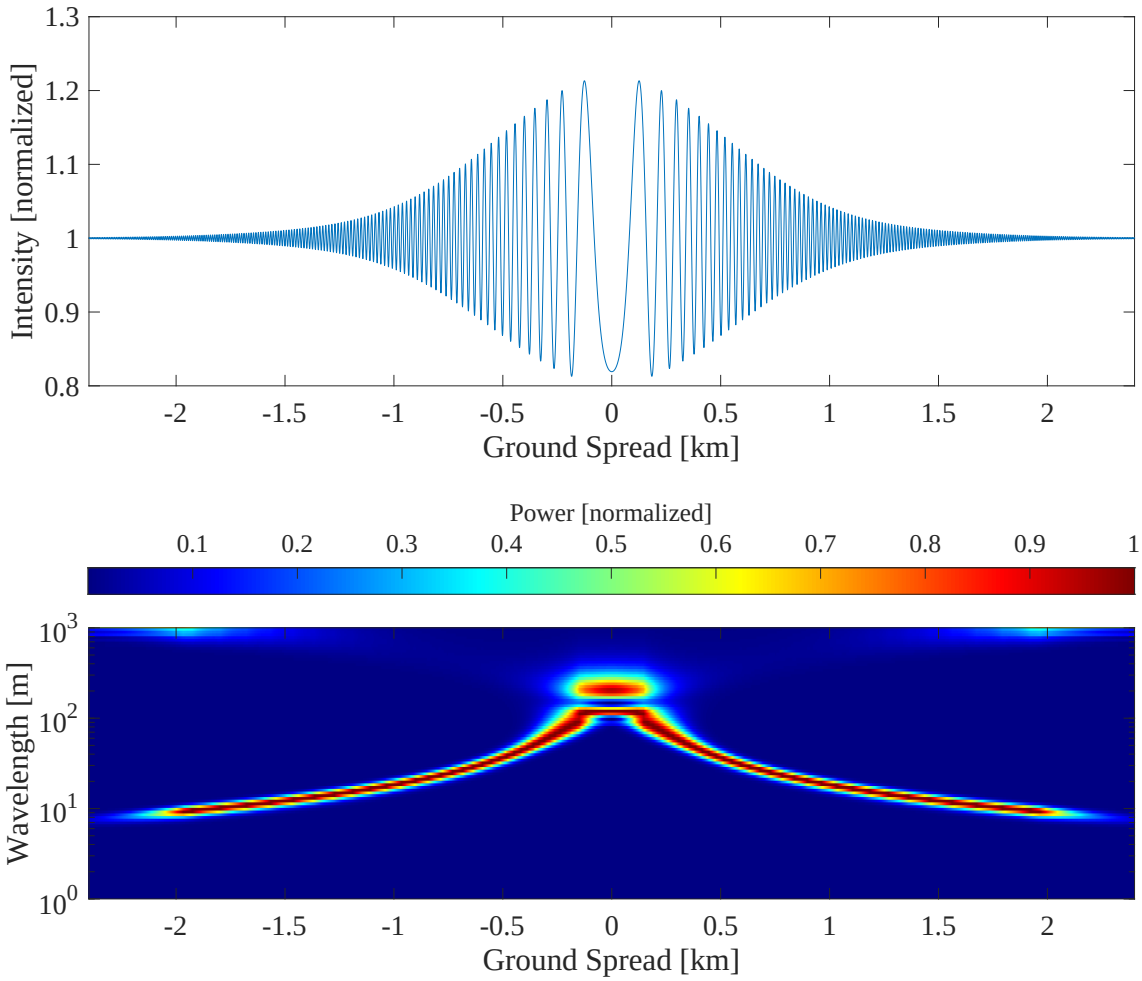

Figure 26. The wavelet spectrogram (PSD as a function of ground spread) of the signal after passing through the trail at an altitude of 81 km with $\phi_0 = -1.1$ rads and $r = 7.5\,m$.

Figure 25 is a power spectrum of the signal and Figure 26 shows the wavelets. Their important features can be found in Table 8.

Table 8. Important results from Stardust's trail at an altitude of 81 km with $\phi_0 = -1.1$ rads and $r = 7.5\,m$

S_4 Max	$= 0.130$
σ_{phi} Max [rad]	$= 0.064$
Peak frequency [1/km]	$= 4.490$

Based on the phase, Stardust's trail would likely be detected by a ground-based

GPS receiver. The phase at the ground plane shown in Figure 24 is for the last detectable time. This means the all the previous times would have a much greater effect on the signal and would also be detectable. With 4.7 seconds of detectable time, Stardust's trail would likely be observed in the data.

3.2.5 Ideal Scenario.

Based on the previous scenarios the ideal scenario for detection of a fireball trail would be at the highest altitude for fireball trail formation with sufficient ionization, in this case 90 km, and would also have a high initial ion density so that the trail has time to diffuse. The initial parameters for the ideal scenario are shown in Table 3 and the resulting ion density profiles over time are shown in Figure 27.

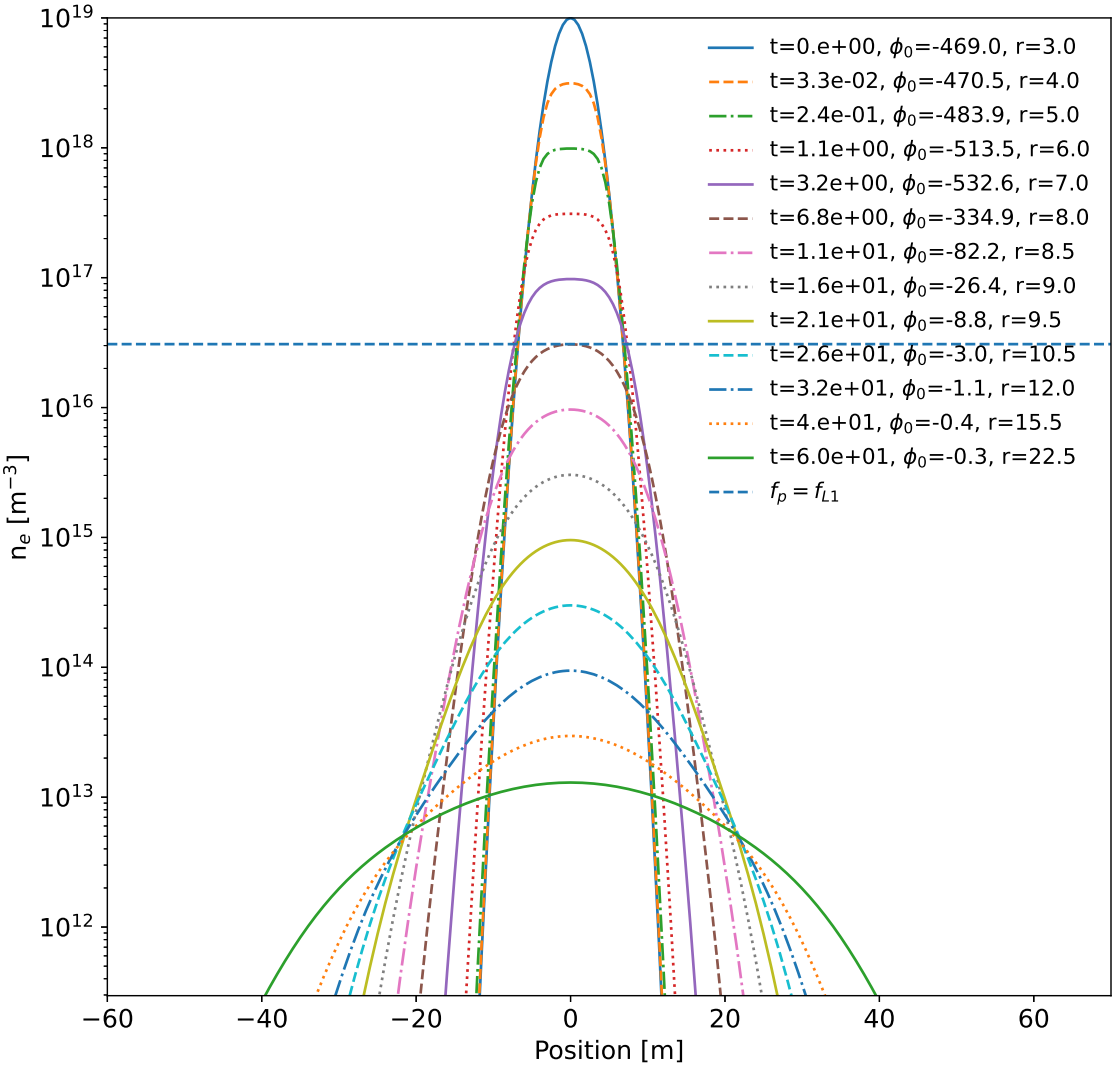

Figure 27. The ion density profile at various times. For each profile a time in seconds, lens strength ϕ_0 in radians, and a trail radius in meters is shown. The dashed line is the point at which the trail's plasma frequency is equal to GPS's L1 frequency.

After 60 seconds the ideal scenario remained above a detectable lens strength. The trails radius starts to grow fast over time as displayed in Figure 27. This is because at later times the peak chemistry loss rate dips below the diffusion loss rate, as displayed in Figure 28. At 60 seconds the lens strength is -0.3 radians and the trail radius is 22.5 m. Figure 29 shows the signal intensity after passing through an ideal trail with the previous parameters.

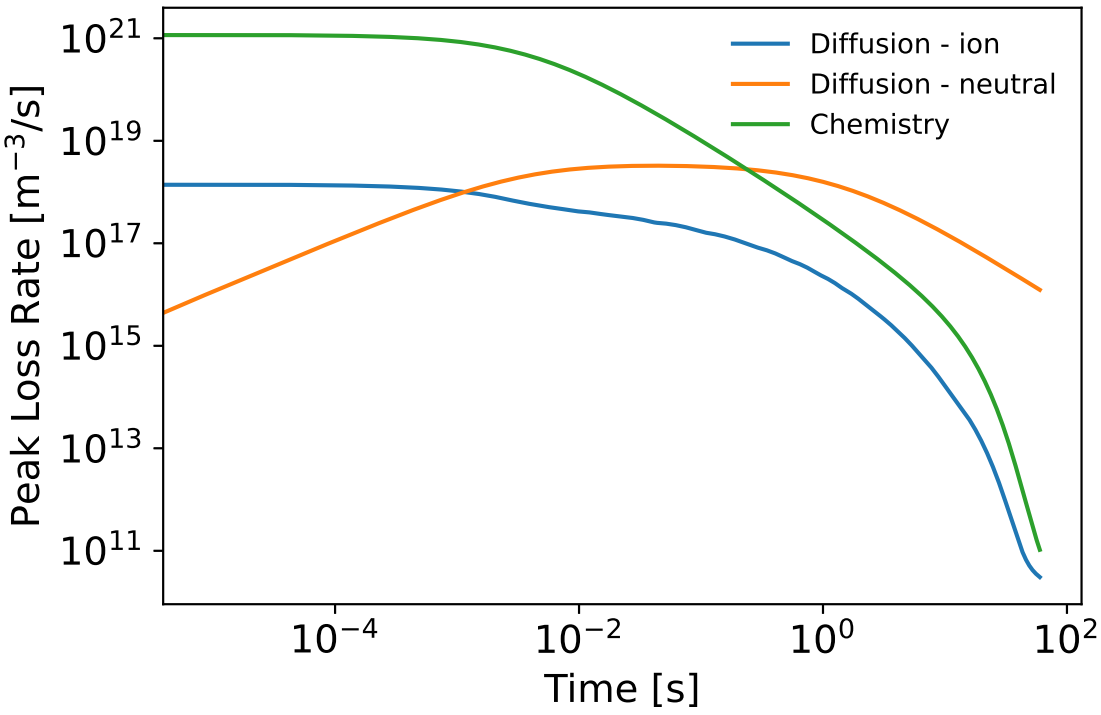

Figure 28. The peak loss rates at the last time step for the Ideal scenario at an altitude of 90 km. The green line is the ion loss rate due to chemistry. The blue line is the ion loss due to the diffusion of ions, and the orange line is the neutral loss rate due to the diffusion of neutrals.

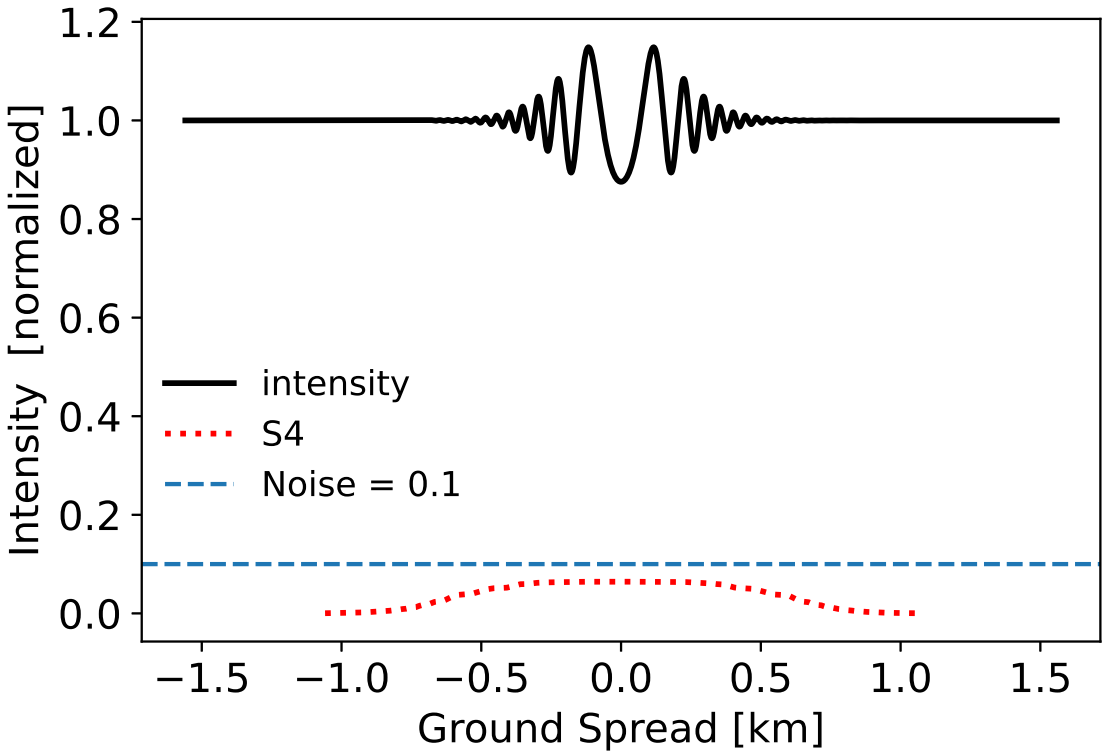

Figure 29. The resulting normalized intensity after passing through the fireball trail at an altitude of 90 km with $\phi_0 = -0.3$ rads and $r = 22.5\,m$. The blue dashed line shows the noise floor and the red dotted line shows the rolling S_4 with a window of 1 km.

This is the first scenario in which the signal's intensity profile is well defined. A symmetric diffraction pattern with a dip in the middle could be a unique pattern in the data, similar to the u-shaped intensity observed for sporadic-E in GPS-RO measurements (6). However, the maximum S_4 is not above the noise floor. Figure 30 shows the phase after passing through an ideal trail.

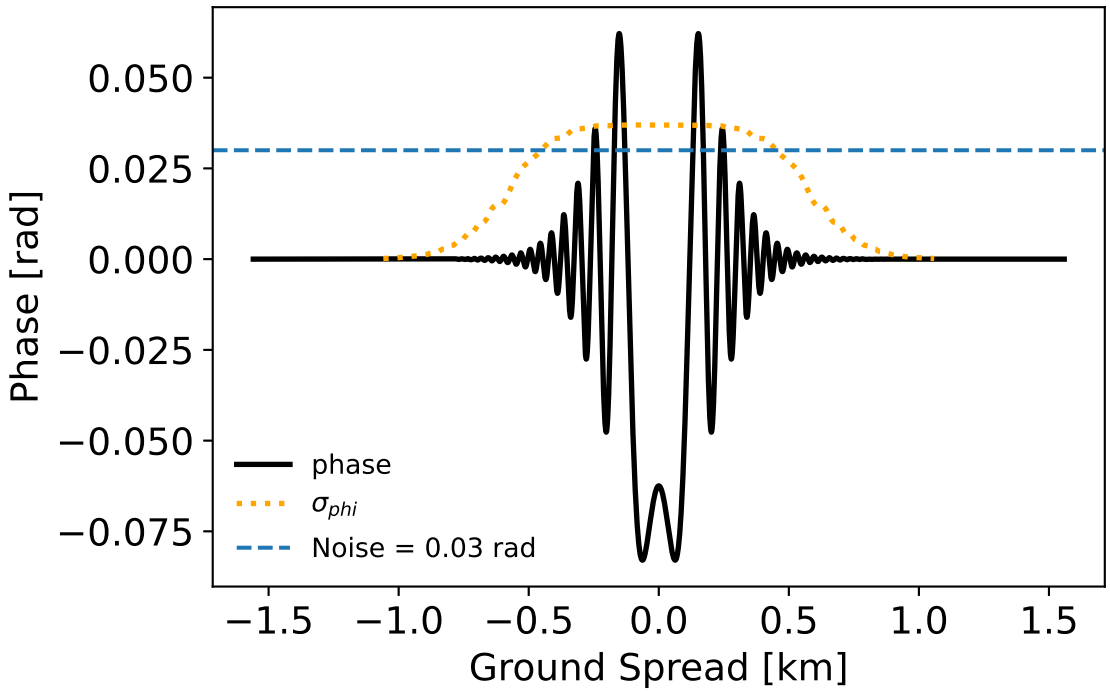

Figure 30. The resulting signal phase after passing through the fireball trail at an altitude of 90 km with $\phi_0 = -0.3$ rads and $r = 22.5\,m$. The blue dashed line shows the noise floor and the yellow dotted line shows the σ_ϕ calculated with a 1 km window.

Figure 30 also shows a distinct symmetric pattern in the phase. The maximum σ_ϕ found in Table 9 is above the noise floor and very pronounced, thus would appear in the data.

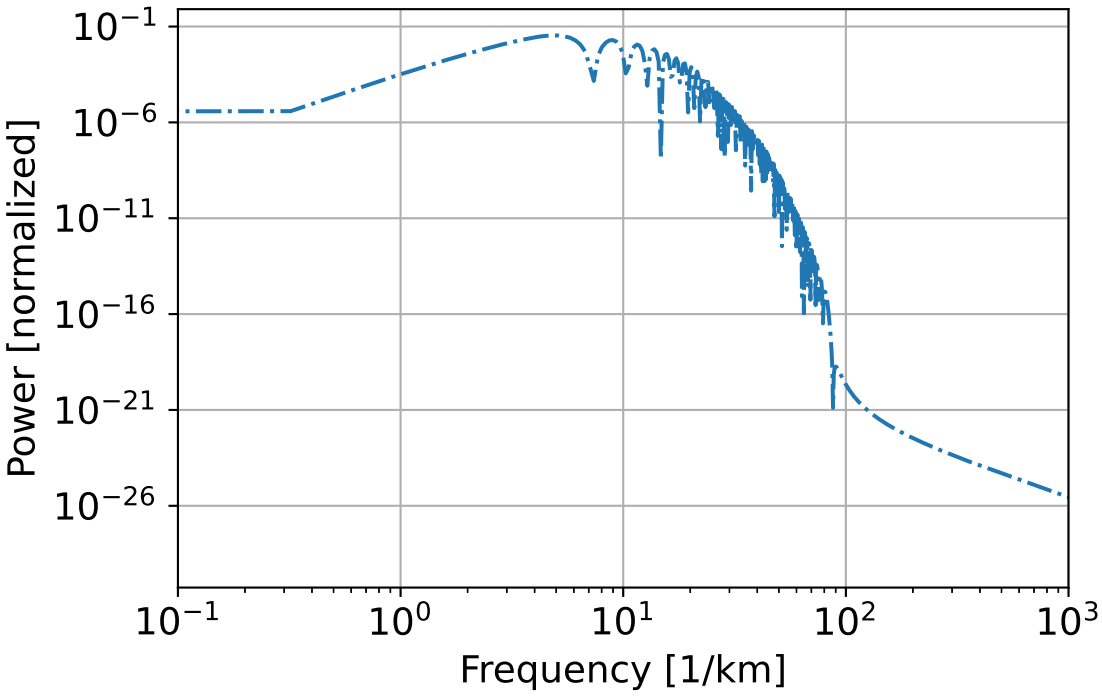

Figure 31. The power spectrum of the signal intensity after passing through the trail at an altitude of 90 km with $\phi_0 = -0.3$ rads and $r = 22.5\,m$.

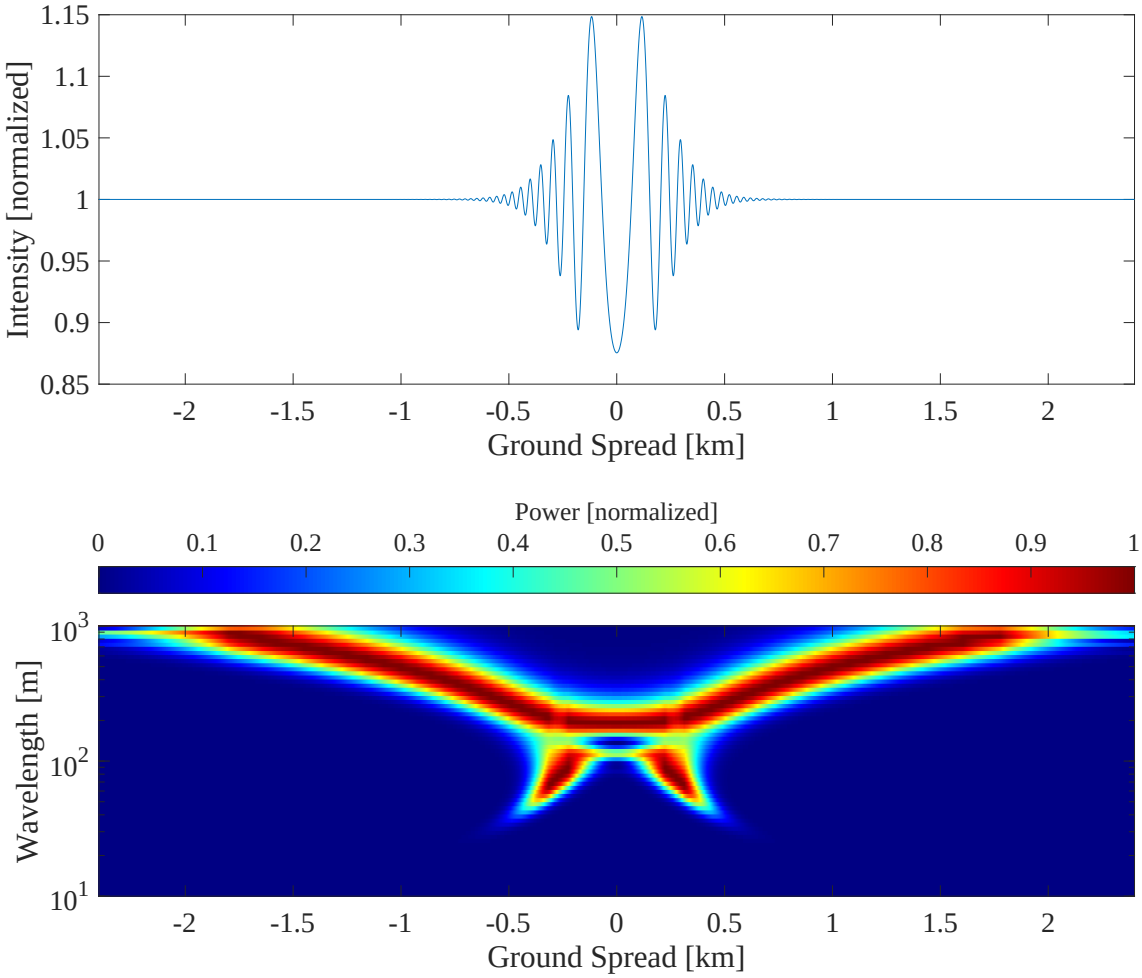

Figure 32. The wavelet spectrogram (PSD as a function of ground spread) of the signal after passing through the trail at an altitude of 90 km with $\phi_0 = -0.3$ rads and $r = 22.5m$.

Figure 31 is a power spectrum of the signal, whose important features can be found in Table 9. Figure 32 shows the wavelets. In this case the wavelet shows a V-shaped chirp. Also this scenario is the first whose S_4 is below the noise floor, thus making the wavelet specrogram a possible useful tool to still detect a fireball using the intensity data.

Table 9. Important results from the ideal trail at an altitude of 90 km with $\phi_0 = -0.3$ rads and $r = 22.5\,m$.

S_4 Max	$= 0.064$
σ_{phi} Max [rad]	$= 0.037$
Peak frequency [1/km]	$= 4.811$

Based on all factors, detection time, S_4, and σ_ϕ the ideal scenario has a high probability of detection by a ground based GPS receiver. It is also not unreasonable to find a fireball with these initial parameters. It's important to note that in all the scenarios looked at, only the last detectable case was used. This last detectable case will always the the closest to not being detected and the least pronounced. What this means is, all time steps before the last detectable case will be even more detectable and more pronounced. This is why in the ideal scenario the S_4 was the worst of all scenarios, while the ideal scenario initial conditions still being the best for detection.

IV. Conclusions

This study analyzed the feasibility of detecting a fireball trail using a ground based GPS receiver. First, the interactions between the meteor trail and ionosphere were modeled including, the predominate interactions of diffusion and recombination providing time dependent ion density profiles at various altitudes. The resulting ion density profiles are used to simulate the perturbation of GPS signals passing through the trail. Through analysis of the resulting signal intensity S_4 and σ_ϕ, detection feasibility can be determined.

For a meteor that is predominately iron with an initial radius of 2 m, five different scenarios were modeled. Each scenario varied the altitude and the initial peak ion density. For the first two scenarios, a fireball at 50 km and the Ram-C reentry vehicle at 60 km, the trail ion densities were reduced to undetectable levels within milliseconds. Given the cadence of a GPS receiver and the GPS signal traverse time, detection times less than a second will not appear in the data, rendering these two scenarios unfeasible for detection.

The third scenario, Apollo capsule at 75 km, had just over one second of detectable ion densities. For the last detectable profile, the S_4 was below the noise floor but σ_ϕ was above the noise floor, thus all ion profiles before this time will be detectable. Apollo was the first scenario to show significant trail diffusion due to its increased altitude, thus increasing the likelihood of detection. This means that the Apollo capsule is the lower bound for initial trail conditions for detection using GPS signals measured at a ground station.

For the forth scenario, Stardust at 81 km, a strong signal lasted 4.7 seconds before dropping below detection and had similar trail diffusion to Ram-C. Also like Ram-C, Stardust's S_4 was too close to the noise floor to be noticed in the data, though its σ_ϕ was above the noise floor and would likely be observed in the data.

Scenario five was a theoretical ideal scenario. Based on the previous four scenarios the major determining factor for detection is altitude. This is because at a high altitude the ion density is not rapidly recombined and the diffusion coefficients are high enough to allow significant trail diffusion. The ideal scenario was at 90 km, the highest altitude with sufficient fireball densities for observation. The results from the ideal scenario showed 60 seconds of detectable ion densities. The resulting GPS signal after passing through a trail with the last ion density profile showed an S_4 above -0.06, which is not above the 0.1 noise floor. However, σ_ϕ was above the noise floor. Although, the S_4 in the ideal scenario was below the noise floor, the wavelet spectrogram of the intensity data reveals a pronounced chirp pattern, which could lead to detection using the intensity data. In conclusion, it is feasible that a fireball trail can be detected by analyzing the resulting amplitude and phase after a GPS signal passes through a meteor trail given that the meteor trail has a sufficiently high initial ion density, above approximately $10^{18}\ m^{-3}$, and occurs at an altitude above approximately 75 km.

There are several future considerations for improving this model. The model could be made more robust by including electric and magnetic effect, thus enabling a greater altitude range. Also, the chemistry could be expanded to include anions which might increase the overall density. Lastly, the model could be expanded to account for a more dynamic atmosphere environment. Including turbulence and wind shear to the trail model. The most prudent extension would be to analyze GEONET GPS data after known fireball sightings to test this simulated feasibility. Also these methods could be applied to different situations other than GPS. Tools like high frequency and very high frequency radars could be used in a similar way.

Bibliography

1. N. Mitchell, "Radar: Meteor radar," in *Encyclopedia of Atmospheric Sciences*, pp. 438–443, Elsevier Academic Press Inc, 2014.

2. Y.-M. Yang, A. Komjathy, R. B. Langley, P. Vergados, M. D. Butala, and A. J. Mannucci, "The 2013 chelyabinsk meteor ionospheric impact studied using gps measurements," *Radio Science*, vol. 49, no. 5, pp. 341–350, 2014.

3. Y. Luo, Y. Yao, and L. Shan, "Analysis of ionospheric disturbances caused by the 2018 bering sea meteor explosion based on gps observations," *Sensors*, vol. 20, no. 11, p. 3201, 2020.

4. J. Maeda, T. Suzuki, M. Furuya, and K. Heki, "Imaging the midlatitude sporadic e plasma patches with a coordinated observation of spaceborne insar and gps total electron content," *Geophysical research letters*, vol. 43, no. 4, pp. 1419–1425, 2016.

5. J. Maeda and K. Heki, "Morphology and dynamics of daytime mid-latitude sporadic-e patches revealed by gps total electron content observations in japan," *Earth, Planets and Space*, vol. 67, no. 1, pp. 1–9, 2015.

6. Z. Zeng and S. Sokolovskiy, "Effect of sporadic e clouds on gps radio occultation signals," *Geophysical Research Letters*, vol. 37, no. 18, 2010.

7. J. Y. Gooch, J. J. Colman, O. A. Nava, and D. J. Emmons, "Global ionosonde and gps radio occultation sporadic-e intensity and height comparison," *Journal of Atmospheric and Solar-Terrestrial Physics*, vol. 199, p. 105200, 2020.

8. D. W. Stambovsky, J. J. Colman, O. A. Nava, and D. J. Emmons, "Simulation of gps radio occultation signals through sporadic-e using the multiple phase

screen method," *Journal of Atmospheric and Solar-Terrestrial Physics*, vol. 214, p. 105538, 2021.

9. K. Igarashi, M. Nakamura, P. Wilkinson, J. Wu, A. Pavelyev, J. Wickert, *et al.*, "Global sounding of sporadic e layers by the gps/met radio occultation experiment," *Journal of Atmospheric and Solar-Terrestrial Physics*, vol. 63, no. 18, pp. 1973–1980, 2001.

10. G. W. Wetherill and C. M. Alexander, "Meteor and meteoroid," *Encyclopedia Britannica*, 2020.

11. Z. Ceplecha, J. Borovička, W. G. Elford, D. O. ReVelle, R. L. Hawkes, V. Porubčan, and M. Šimek, "Meteor phenomena and bodies," *Space Science Reviews*, vol. 84, no. 3, pp. 327–471, 1998.

12. K. Yomogida and T. Matsui, "Physical properties of ordinary chondrites," *Journal of Geophysical Research: Solid Earth*, vol. 88, no. B11, pp. 9513–9533, 1983.

13. J. M. C. Plane, "Atmospheric chemistry of meteoric metals," *Chemical Reviews*, vol. 103, no. 12, pp. 4963–4984, 2003.

14. R. Schunk and A. Nagy, *Ionospheres: physics, plasma physics, and chemistry*. Cambridge university press, 2009.

15. "Gps.gov: Space segment," 2021.

16. H. Tsuji, Y. Hatanaka, Y. Hiyama, K. Yamaguchi, T. Furuya, S. Kawamoto, and Y. Fukuzaki, "Twenty-year successful operation of GEONET," *Bulletin of the Geospatial Information Authority of Japan*, vol. 65, p. 20, 2017.

17. R. Buckley, "Diffraction by a random phase-changing screen: A numerical experi-

ment," *Journal of Atmospheric and Terrestrial Physics*, vol. 37, no. 11, pp. 1431–1446, 1975.

18. T. Barlyaeva, T. Barata, and A. Morozova, "Datasets of ionospheric parameters provided by SCINDA GNSS receiver from Lisbon airport area," *Data in Brief*, vol. 31, p. 105966, 2020.

19. E. de Paula, A. Martinon, A. Moraes, C. Carrano, A. Neto, P. Doherty, K. Groves, C. Valladares, G. Crowley, I. Azeem, *et al.*, "Performance of 6 different global navigation satellite system receivers at low latitude under moderate and strong scintillation," *Earth and Space Science*, vol. 8, no. 2, p. e2020EA001314, 2021.

20. D. Bilitza, D. Altadill, V. Truhlik, V. Shubin, I. Galkin, B. Reinisch, and X. Huang, "International reference ionosphere 2016: From ionospheric climate to real-time weather predictions," *Space weather*, vol. 15, no. 2, pp. 418–429, 2017.

21. J. MacDougall, J. Plane, and P. Jayachandran, "Polar cap sporadic-E: part 2, modeling," *Journal of Atmospheric and Solar-Terrestrial Physics*, vol. 62, no. 13, pp. 1169–1176, 2000.

22. M. Baeva, D. Uhrlandt, and A. B. Murphy, "A collisional-radiative model of iron vapour in a thermal arc plasma," vol. 50, p. 22LT02, may 2017.

23. W. Baggaley and C. Cummack, "Meteor train ion chemistry," *Journal of Atmospheric and Terrestrial Physics*, vol. 36, no. 11, pp. 1759–1773, 1974.

24. X. Chu and Z. Yu, "Formation mechanisms of neutral fe layers in the thermosphere at antarctica studied with a thermosphere-ionosphere fe/fe+ (tife) model," *Journal of Geophysical Research: Space Physics*, vol. 122, no. 6, pp. 6812–6848, 2017.

25. T. Nygren, L. Jalonen, J. Oksman, and T. Turunen, "The role of electric field and neutral wind direction in the formation of sporadic e-layers," *Journal of atmospheric and terrestrial physics*, vol. 46, no. 4, pp. 373–381, 1984.

26. R. Courant, K. Friedrichs, and H. Lewy, "On the partial difference equations of mathematical physics," *IBM journal of Research and Development*, vol. 11, no. 2, pp. 215–234, 1967.

27. J. Zhong, T. Ozawa, and D. A. Levin, "Modeling of stardust reentry ablation flows in the near-continuum flight regime," *AIAA journal*, vol. 46, no. 10, pp. 2568–2581, 2008.

28. J. Borovicka, "A fireball spectrum analysis," *Astronomy and Astrophysics*, vol. 279, pp. 627–645, 1993.

29. J. Picone, A. Hedin, D. P. Drob, and A. Aikin, "Nrlmsise-00 empirical model of the atmosphere: Statistical comparisons and scientific issues," *Journal of Geophysical Research: Space Physics*, vol. 107, no. A12, pp. SIA–15, 2002.

30. J. Jones, B. McIntosh, and M. Simek, "Ozone and the duration of overdense radio meteors," *Journal of atmospheric and terrestrial physics*, vol. 52, no. 4, pp. 253–258, 1990.

REPORT DOCUMENTATION PAGE

Form Approved
OMB No. 0704–0188

1. REPORT DATE *(DD–MM–YYYY)*	2. REPORT TYPE	3. DATES COVERED *(From — To)*
21–03–2022	Master's Thesis	May 2020 — Mar 2022

4. TITLE AND SUBTITLE

FEASIBILITY OF FIREBALL TRAIL DETECTION USING GROUND-BASED GPS RECEIVERS

5a. CONTRACT NUMBER

5b. GRANT NUMBER

5c. PROGRAM ELEMENT NUMBER

6. AUTHOR(S)

Moffett, Ian Robert, 2d Lt, USAF

5d. PROJECT NUMBER

5e. TASK NUMBER

5f. WORK UNIT NUMBER

7. PERFORMING ORGANIZATION NAME(S) AND ADDRESS(ES)

Air Force Institute of Technology
Graduate School of Engineering and Management (AFIT/EN)
2950 Hobson Way
WPAFB OH 45433-7765

8. PERFORMING ORGANIZATION REPORT NUMBER

AFIT-ENP-MS-22-M-100

9. SPONSORING / MONITORING AGENCY NAME(S) AND ADDRESS(ES)

Air Force Research Laboratory
2241 Avionics Circle
WPAFB, OH 45433
COMM (937) 713-8550
Email: james.caplinger.1@us.af.mil

10. SPONSOR/MONITOR'S ACRONYM(S)

AFRL/RY

11. SPONSOR/MONITOR'S REPORT NUMBER(S)

12. DISTRIBUTION / AVAILABILITY STATEMENT

DISTRIBUTION STATEMENT A:
APPROVED FOR PUBLIC RELEASE; DISTRIBUTION UNLIMITED.

13. SUPPLEMENTARY NOTES

14. ABSTRACT

The feasibility of using GPS data to detect fireballs is analyzed by first modeling the fireball's trail diffusion and plasma chemistry to get a resulting ion density profile of the trail over time. The signal perturbation caused by the fireball trail is simulated for a ground receiver using an analytic solution for diffraction from a Gaussian lens. Five cases were modeled with varying initial peak ion densities and altitudes taken from fireball and reentry vehicle data. This paper shows that it is feasible to detect a fireball trail using GPS if the fireball has a sufficiently high initial ion density, above approximately $10^{18}\ m^{-3}$, and occurs at an altitude above approximately 75 km. For the five cases the amplitude scintillation index, S_4, and phase scintillation index, σ_ϕ, values of the signal for the last detectable ion density profile were calculated.

15. SUBJECT TERMS

Fireball, GPS, Ionosphere, Detection

16. SECURITY CLASSIFICATION OF:			17. LIMITATION OF ABSTRACT	18. NUMBER OF PAGES	19a. NAME OF RESPONSIBLE PERSON
a. REPORT	b. ABSTRACT	c. THIS PAGE			Maj Daniel J. Emmons, AFIT/ENP
U	U	U	U	69	19b. TELEPHONE NUMBER *(include area code)* (937) 255-3636, x4571; Daniel.Emmons@afit.edu